NASA TM X-534

TECHNICAL MEMORANDUM

X-534

INVESTIGATION OF THE LOW SUBSONIC STABILITY AND CONTROL CHARACTERISTICS OF A MODEL OF A HYPERSONIC BOOST-GLIDE AIRPLANE DESIGNED FOR HIGH LIFT-DRAG RATIOS AT LOW SPEEDS

By George M. Ware and Robert E. Shanks

Langley Research Center
Langley Field, Va.

NATIONAL AERONAUTICS AND SPACE ADMINISTRATION
WASHINGTON June 1961

NATIONAL AERONAUTICS AND SPACE ADMINISTRATION

TECHNICAL MEMORANDUM X-534

INVESTIGATION OF THE LOW SUBSONIC STABILITY AND CONTROL CHARACTERISTICS OF A MODEL OF A HYPERSONIC BOOST-GLIDE AIRPLANE DESIGNED FOR HIGH LIFT-DRAG RATIOS AT LOW SPEEDS*

By George M. Ware and Robert E. Shanks

SUMMARY

An investigation has been made to measure the low-speed static longitudinal and lateral stability and control characteristics and lateral damping derivatives of a model of a hypersonic boost-glide airplane designed for high lift-drag ratios at low speeds. Included in the investigation were tests to determine the effects of various configuration changes on the static stability characteristics and lift-drag ratio of the model.

The results indicated that the model was longitudinally stable about the design center-of-gravity position (55.7 percent of the body length) except for the angle-of-attack range from about 15° to 20°. The maximum trimmed lift-drag ratio of the basic model was approximately 6.0. Tests indicated that the model had positive directional stability up to an angle of attack of 35° and had positive damping in roll and yaw throughout the angle-of-attack range tested (0° to 50°).

INTRODUCTION

An investigation has been conducted by the National Aeronautics and Space Administration to provide information on proposed hypersonic boost-glide airplane configurations from hypersonic to low subsonic speeds. The results of a series of tests conducted over a Mach number range from 0.04 to 9.6 at the Langley Research Center on several configurations of one proposed boost-glide airplane have been reported in references 1 to 9.

The present investigation was made to determine the low subsonic speed static longitudinal and lateral stability and control characteristics and lateral damping derivatives of one of the configurations studied. This particular model, which was designed to give a relatively high lift-drag ratio at low speeds, had a 70° swept wing with a thick cambered airfoil, a large teardrop-shaped fuselage with a small base area, and wing-tip vertical tails.

The investigation consisted of force tests at angles of attack from 0° to 40° to determine the static longitudinal and lateral characteristics for the basic model and for the model with various modifications, and oscillation tests at angles of attack from 0° to 50° to determine the lateral damping derivatives for the basic model. The modifications studied included a change in wing trailing-edge sweep, increased wing-body fairing, a cutout in the forward leading edge of the wing, vertical-tail cant, addition of horizontal fins, wing leading-edge extensions, wing fences, and landing skids.

SYMBOLS

The longitudinal data are referred to the wind axes and all lateral stability data are referred to the body system of axes (see fig. 1) originating at a moment reference position of 55.7 percent of the body length (for corresponding percent of the mean aerodynamic chords, see table I) for all configurations. All measurements are reduced to standard coefficient form and are presented in terms of the following symbols:

b	wing span, ft
$\bar{c}$	mean aerodynamic chord, ft
D	drag, lb
f	frequency of oscillations, cps
F_Y	side force, lb
k	reduced-frequency parameter, $\omega b/2V$
L	lift, lb
L/D	lift-drag ratio
M_X	rolling moment, ft-lb

M_Y	pitching moment, ft-lb
M_Z	yawing moment, ft-lb
p	rolling velocity, radians/sec
$\dot{p} = \frac{dp}{dt}$	
q	free-stream dynamic pressure, lb/sq ft
r	yawing velocity, radians/sec
$\dot{r} = \frac{dr}{dt}$	
S	wing area, sq ft
t	time, sec
V	free-stream velocity, ft/sec
X, Y, Z	body reference axes unless otherwise noted
α	angle of attack, deg
β	angle of sideslip, deg or radians
$\dot{\beta} = \frac{d\beta}{dt}$	
δ_a	aileron deflections, $\delta_{e,R} - \delta_{e,L}$, deg
δ_e	elevator deflection (positive when trailing edge down), deg
$\delta_{e,L}$	left elevon deflection (positive when trailing edge down), deg
$\delta_{e,R}$	right elevon deflection (positive when trailing edge down), deg
$\delta_{r,R}$	right rudder deflection (outward only, measured from vertical tail center line), deg
ϕ	angle of roll, radians
ψ	angle of yaw, radians

$\omega = 2\pi f$ radians/sec

C_D drag coefficient, $\frac{D}{qS}$

C_l rolling-moment coefficient, $\frac{M_X}{qSb}$

ΔC_l incremental rolling-moment coefficient

$C_{l_\beta} = \frac{\partial C_l}{\partial \beta}$ per degree or per radian

C_L lift coefficient, $\frac{L}{qS}$

C_m pitching-moment coefficient, $\frac{M_Y}{qS\bar{c}}$

C_n yawing-moment coefficient, $\frac{M_Z}{qSb}$

ΔC_n incremental yawing-moment coefficient

$C_{n_\beta} = \frac{\partial C_n}{\partial \beta}$ per degree or per radian

C_Y side-force coefficient, $\frac{F_Y}{qS}$

$C_{Y_\beta} = \frac{\partial C_Y}{\partial \beta}$ per degree or per radian

$$C_{l_r} = \frac{\partial C_l}{\partial \frac{rb}{2V}} \qquad C_{n_r} = \frac{\partial C_n}{\partial \frac{rb}{2V}} \qquad C_{Y_r} = \frac{\partial C_Y}{\partial \frac{rb}{2V}}$$

$$C_{l_p} = \frac{\partial C_l}{\partial \frac{pb}{2V}} \qquad C_{n_p} = \frac{\partial C_n}{\partial \frac{pb}{2V}} \qquad C_{Y_p} = \frac{\partial C_Y}{\partial \frac{pb}{2V}}$$

$$C_{l_{\dot\beta}} = \frac{\partial C_l}{\partial \frac{\dot\beta b}{2V}} \qquad C_{n_{\dot\beta}} = \frac{\partial C_n}{\partial \frac{\dot\beta b}{2V}} \qquad C_{Y_{\dot\beta}} = \frac{\partial C_Y}{\partial \frac{\dot\beta b}{2V}}$$

$$C_{l_{\dot r}} = \frac{\partial C_l}{\partial \frac{\dot r b}{2V}} \qquad C_{n_{\dot r}} = \frac{\partial C_n}{\partial \frac{\dot r b}{2V}} \qquad C_{Y_{\dot r}} = \frac{\partial C_Y}{\partial \frac{\dot r b}{2V}}$$

$$C_{l_{\dot p}} = \frac{\partial C_l}{\partial \frac{\dot p b}{2V}} \qquad C_{n_{\dot p}} = \frac{\partial C_n}{\partial \frac{\dot p b}{2V}} \qquad C_{Y_{\dot p}} = \frac{\partial C_Y}{\partial \frac{\dot p b}{2V}}$$

DEFINITION OF DERIVATIVES

The term "in-phase derivative" used herein refers to any one of the stability derivatives which are based on the forces or moments in phase with the angle of roll or yaw produced in the oscillatory tests. The term "out-of-phase derivative" refers to any one of the stability derivatives which are based on the forces or moments 90° out of phase with the angle of roll or yaw. The derivatives were measured in the oscillation tests in the following combinations:

In-phase rolling derivatives:

$$C_{l_\beta} \sin \alpha - k^2 C_{l_{\dot{p}}}$$

$$C_{n_\beta} \sin \alpha - k^2 C_{n_{\dot{p}}}$$

$$C_{Y_\beta} \sin \alpha - k^2 C_{Y_{\dot{p}}}$$

In-phase yawing derivatives:

$$C_{l_\beta} \cos \alpha + k^2 C_{l_{\dot{r}}}$$

$$C_{n_\beta} \cos \alpha + k^2 C_{n_{\dot{r}}}$$

$$C_{Y_\beta} \cos \alpha + k^2 C_{Y_{\dot{r}}}$$

Out-of-phase rolling derivatives:

$$C_{l_p} + C_{l_{\dot{\beta}}} \sin \alpha$$

$$C_{n_p} + C_{n_{\dot{\beta}}} \sin \alpha$$

$$C_{Y_p} + C_{Y_{\dot{\beta}}} \sin \alpha$$

Out-of-phase yawing derivatives:

$$C_{l_r} - C_{l_{\dot{\beta}}} \cos \alpha$$

$$C_{n_r} - C_{n_{\dot{\beta}}} \cos \alpha$$

$$C_{Y_r} - C_{Y_{\dot{\beta}}} \cos \alpha$$

APPARATUS AND MODELS

The static and rotary oscillation tests were conducted at the Langley Research Center in a low-speed tunnel with a 12-foot octagonal test section. Detailed descriptions of the oscillation apparatus and methods used in obtaining and reducing the data are given in reference 10. The model was sting mounted and the forces and moments were measured about the body axes by means of three-component internal strain-gage balances.

A three-view drawing of the model used in the investigation is presented in figure 2 and photographs of the model are presented in figure 3. The various configurations of this series of hypersonic boost-glide airplanes are identified by numerical subscripts to letters indicating model components: B for body, W for wing, and V for vertical tail. (See refs. 1 to 9.) Sketches of the modifications to the model are presented in figure 4 and include: two elevons that were interchangeable with the original elevons to give wing trailing-edge sweep angles of 36.8° (designated W_{8A}) and 0° (designated W_{8B}), a cutout in the wing leading edge at the wing-fuselage juncture, horizontal fins extending out from the vertical tails, removable landing skids, wing leading-edge extensions extending 40 percent or 60 percent of the semispan inboard of the wing tip, several wing fences located either on the inboard or outboard portion of the wing, and an increased wing-body fairing. The model was constructed so that the tails could be canted outward 30° from the vertical or removed.

L 1330

TESTS

The static longitudinal and lateral stability characteristics of the model and its modifications were determined for an angle-of-attack range of 0° to 40°. The lateral characteristics were determined from tests made at various angles of attack over a sideslip range of -20° to 20°. Rolling and yawing oscillation tests were made over an angle-of-attack range from 0° to 50°. These rotary oscillation tests were made at reduced-frequency parameters of 0.10 and 0.17 for amplitudes in roll and yaw of $\pm 5^\circ$.

The tests were made at a dynamic pressure of 4.09 pounds per square foot which corresponds to an airspeed of 58.7 feet per second and a test Reynolds number of 0.373×10^6 per foot or 1.09×10^6 based on the mean aerodynamic chord of W_8.

RESULTS AND DISCUSSION

Longitudinal Characteristics

The data in figures 5 and 6 show the characteristics of the basic model while the data in figures 7 to 13 show the effect of various model modifications which were made in an effort to improve longitudinal stability and lift-drag ratios. The lift-drag ratio comparisons made herein are for the untrimmed condition ($\delta_e = 0^\circ$) unless otherwise noted.

Effect of elevator deflection. - The effect of elevator deflection on the longitudinal characteristics on model $B_8W_8V_{10}$ is presented in figure 5. These data show that the model was approximately neutrally stable up to about an angle of attack of 15°, unstable at angles of attack from 15° to 20°, and generally stable at angles of attack from 20° to 40°. Elevator deflection had an appreciable effect on the shape of the pitching-moment curve in that upward (negative) deflection reduced the instability in the angle-of-attack range from 15° to 20° and downward deflection increased this instability. The elevator effectiveness remained constant up to an angle of attack of 20° and then decreased with increasing angle of attack. It should be pointed out that a rather large elevator deflection ($\delta_e \approx -10^\circ$) was required to trim the model at angles of attack up to 15°. The model had a maximum lift-drag ratio of 6.6 with an elevator deflection of 0° but dropped to about 6.0 with an up-elevator deflection of 10° (approximate trimmed condition from $\alpha = 0$ to $\alpha = 15^\circ$).

Effect of landing skids. - The effect of landing skids on the longitudinal characteristics of the model is presented in figure 6. These data show that the addition of skids resulted in a slight increase in longitudinal stability and a decrease in maximum lift and lift-drag ratio.

Wing trailing-edge configuration. - From the data presented in figure 7 it may be seen that, with the center of gravity located at 55.7 percent of the body length, the stability of the model was increased as additional area was added to the wing by decreasing the trailing-edge sweep (W_{8B}) and decreased by increasing the trailing-edge sweep (W_{8A}). The change in stability was most apparent in the angle-of-attack range from 20° to 40°. Although the pitching-moment curve became more nearly linear with an increase in stability in this range, the model still remained unstable at angles of attack from 15° to 20°. The various wing trailing-edge configurations had some effect on the lift-curve slope but compensating changes in drag resulted in almost no change in maximum lift-drag ratio.

[redacted]

Horizontal fins.- The effect of the horizontal fins which were designed to fold out from the vertical tails at low speeds (see fig. 4(a)) is presented in figure 8. These data show that the fins increased the static margin by about $0.05\bar{c}$ up to an angle of attack of 15°. The lift coefficient was also increased slightly up to about $\alpha = 20^\circ$ whereas above an angle of attack of 20° the lift coefficients were reduced slightly, apparently because the horizontal fins were stalled by the upwash at the wing tips of the model. The data also show that the fins had only a slight effect on the maximum lift-drag ratio.

Leading-edge extensions.- The particular wing leading-edge extensions used in this investigation had a destabilizing effect and resulted in the model being unstable even at low angles of attack as shown in figure 9. The maximum lift-drag ratio of the 40-percent b/2 leading-edge extension configuration was lower than that of the basic model probably because of an unfavorable location of the extension which caused an increase in drag without an appropriate increase in lift. When the extension was increased to cover 60 percent of the wing leading edge, the lift-drag ratio was increased to about 7.2 which was an improvement of 0.6 over that of the basic model.

L
1
3
3
0

Vertical-tail cant.- The data in figure 10 show that canting the vertical tails out 30° from the vertical increased the stability but did not eliminate the instability in the angle-of-attack range from 15° to 20°. Canting the tails out also resulted in a large negative shift in the pitching-moment curve. Data for the model with vertical tails removed are also presented in figure 10 and show that removing the tails shifted the pitching-moment curve in a positive direction and resulted in a fairly linear curve. There was also a small reduction in stability up to an angle of attack of 15° with tails off. Analyzing the data in this figure in an effort to determine the cause of the instability in the angle-of-attack range from 15° to 20° leads to the conclusion that the vertical tails, acting as endplates, increased the effectiveness of the rear portion of the wing at low angles of attack which added a nose-down increment to the pitching-moment curve. At an angle of attack of about 15°, regardless of tail configuration, the flow over the rear of the wing probably separated and caused a loss in lift over that portion of the wing; thus the model became unstable. The maximum L/D ratio of the tails-off configuration may be seen to be 7.0. Canting the tails out 30° from the vertical increased the lift coefficients over the test angle-of-attack range and increased the maximum L/D ratio to about 8.5.

Wing-body fairing.- As may be seen from the data in figure 11, the wing-body fairing slightly increased the stability of the model at the lower angles of attack and was effective in reducing the instability in the angle-of-attack range from 15° to 20°. The fairing had no appreciable effect on the other longitudinal characteristics.

[redacted]

Wing leading-edge cutout.- A cutout in the wing leading edge at the wing-fuselage juncture (fig. 12) completely eliminated the instability in the angle-of-attack range from 15° to 20° for approximately trimmed conditions ($\delta_e = -10°$). The cutout had no appreciable effect on the value of the maximum L/D ratio but caused a reduction in the maximum lift coefficient and shifted the angle of attack at which the maximum lift-drag ratio occurred from $\alpha = 5°$ to about $\alpha = 8°$.

Wing fences.- The data in figure 13 show that the addition of either the large or the small fences reduced both the maximum lift and the maximum lift-drag ratio of the basic configuration. The fences had no effect on longitudinal stability throughout the angle-of-attack range tested except for a reduction in the instability between angles of attack of 15° and 20°.

Lateral Characteristics

The variation of C_Y, C_n, and C_l with β for various angles of attack is shown in figure 14 for model $B_8W_8V_{10}$ with vertical tails on and off, with landing skids, tails canted out 30° from the vertical, and rudders deflected 20° outward. These tests were made with an elevator deflection of -10° which gave approximately longitudinal trimmed conditions up to an angle of attack of about 15°. These data are summarized in figures 15 to 18 in the form of the stability derivatives C_{Y_β}, C_{n_β}, and C_{l_β} plotted against angle of attack. The values of the derivatives were obtained by taking the difference between the values of the coefficients measured at sideslip angles of 5° and -5°. Since some of the data are nonlinear, these derivatives should be used only to indicate trends and to provide approximate comparison of the various configurations. No lateral tests were made for the model with trailing-edge sweep of 0° and 36.8°, horizontal fins, wing leading-edge extensions, or wing fences because it was felt that these modifications would have little effect on the lateral characteristics of the model. Lateral tests were made, however, for the model with increased wing-body fairing and wing leading-edge cutout and showed almost no change from the characteristics of the basic model.

Effect of vertical tails.- The data presented in figure 15 show that, with vertical tails on, the model was directionally stable up to an angle of attack of about 35°. With the vertical tails off, the model was unstable throughout the test angle-of-attack range and had about the same variation in C_{n_β} with angle of attack as the complete model. The effective dihedral $-C_{l_\beta}$ became increasingly positive up to an angle of attack of about 15° and then decreased and changed sign near an angle of attack of 30°. Points giving the characteristics of model $B_8W_8V_{10}$

with 0° elevator deflection are given in figure 15. The points agree very closely with values obtained with $\delta_e = -10°$; therefore, the lateral characteristics are not greatly affected by moderate negative elevator deflection.

Effect of landing skids.- It may be seen from the data of figure 16 that the landing skids slightly increased the directional stability of the model at low and high angles of attack.

Vertical-tail cant.- The data of figure 17 show that rotating the tails 30° from the vertical, which reduced the effective side area of the tails, decreased the directional stability of the model throughout the test angle-of-attack range. Although the directional stability was reduced, the model still retained some stability up to an angle of attack of 30°.

Symmetrical rudder deflection.- The effect of simultaneous outward deflection of both rudders, which has been suggested as a means of improving directional stability at hypersonic speeds, is shown in figure 18 for the low-speed case. The data show that symmetric rudder deflections of 20° did not change the level of directional stability of the model but eliminated the directional instability at an angle of attack of 35°.

Rudder and aileron effectiveness.- The rudder and aileron control effectiveness of the model is shown in figure 19. The rudder effectiveness remained approximately constant up to an angle of attack of about 15° and decreased with increasing angle of attack to about one-third of the original value at $\alpha = 40°$. The aileron control followed the same trend but maintained constant effectiveness up to an angle of attack of about 25°. Some adverse rolling and yawing moments were produced by the rudder and aileron, respectively, but they were generally small.

Oscillatory Lateral Stability Characteristics

The variation of the out-of-phase yawing and rolling derivatives with angle of attack for model $B_8W_8V_{10}$ is presented in figure 20. These data show that the damping derivatives $C_{n_r} - C_{n_{\dot{\beta}}} \cos \alpha$ and $C_{l_p} + C_{l_{\dot{\beta}}} \sin \alpha$ for the model with vertical tails are negative (stable) throughout the angle-of-attack range tested. Removal of the vertical tails had little effect on $C_{l_p} + C_{l_{\dot{\beta}}} \sin \alpha$ up to an angle of attack of about 20° but with tails off $C_{n_r} - C_{n_{\dot{\beta}}} \cos \alpha$ was about zero or positive over most of the angle-of-attack range. The data show that frequency affects the values of the derivatives, particularly in the higher angle-of-attack range, but generally did not change the trends.

The variation of the in-phase rolling and yawing derivatives for model $B_8W_8V_{10}$ with angle of attack is presented in figure 21. Static stability data ($k = 0$) from figure 14 are also plotted in this figure for correlation with the oscillation test results. The data show fairly good agreement except for the effective dihedral derivatives $C_{l_\beta} \sin \alpha - k^2 C_{l_{\dot{p}}}$ and $C_{l_\beta} \cos \alpha + k^2 C_{l_{\dot{r}}}$, at the higher angles of attack. These differences in the static and oscillatory data may be attributed to flow separation over the wings at high angles of attack and are consistent with results reported in reference 11.

SUMMARY OF RESULTS

The results of the investigation to determine the low subsonic stability characteristics of a model of a hypersonic boost-glide airplane designed for high lift-drag ratio at low speeds are summarized as follows:

1. The model was longitudinally stable about the design center-of-gravity position (55.7 percent of the body length) except in the angle-of-attack range from 15° to 20°.

2. The basic model had a maximum lift-drag ratio of 6.6 with an elevator deflection of 0° and a maximum lift-drag ratio of the order of 6.0 with an elevator deflection of -10° which corresponded to the approximate longitudinal trim condition at low angles of attack.

3. The model was directionally stable up to an angle of attack of 35°.

4. The model had positive damping in roll and in yaw throughout the angle-of-attack range (0° to 50°).

Langley Research Center,
National Aeronautics and Space Administration,
Langley Field, Va., March 6, 1961.

[redacted]

REFERENCES

1. West, F. E., Jr., Trescot, Charles D., Jr., and Wiley, Alfred N., Jr.: Aerodynamic Characteristics for Two Hypersonic Glider Models With and Without Wing and Vertical-Tail Trailing-Edge Chord-Extensions at a Mach Number of 0.94. NASA TM X-66, 1960.

2. Shanks, Robert E.: Effect of Wing Crank and Sweepback on the Low-Subsonic Stability and Control Characteristics of a Model of a Hypersonic Boost-Glide Type Airplane. NASA TM X-181, 1960.

3. West, F. E., Jr., Trescot, Charles D., Jr., and Wiley, Alfred N., Jr.: Effect of Vertical-Tail and Rudder Deflection on the Aerodynamic Characteristics of a Hypersonic Glider Model at Mach Numbers of About 0.62 and 0.93. NASA TM X-189, 1960.

4. Trescot, Charles D., Jr., West, F. E., Jr., and Wiley, Alfred N., Jr.: Effects of Elevon Deflection on the Aerodynamic Characteristics of a Hypersonic Glider Model at Mach Numbers of About 0.62 and 0.96. NASA TM X-203, 1960.

5. West, F. E., Jr., Trescot, Charles D., Jr., and Wiley, Alfred N., Jr.: High Subsonic Investigation of the Aerodynamic Characteristics of a Hypersonic Glider Model With and Without Deflected Elevons and Body Flap. NASA TM X-204, 1960.

6. Ladson, Charles L., Johnston, Patrick J., and Trescot, Charles D., Jr.: Effects of Wing Plan-Form Geometry on the Aerodynamic Characteristics of a Hypersonic Glider at Mach Numbers Up to 9.6. NASA TM X-286, 1960.

7. Ladson, Charles L., and Johnston, Patrick J.: Aerodynamic Characteristics of Two Winged Reentry Vehicles at Supersonic and Hypersonic Speeds. NASA TM X-346, 1961.

8. Ladson, Charles L., and Johnston, Patrick J.: Aerodynamic Characteristics of a Blunt-Nosed Winged Reentry Vehicle at Supersonic and Hypersonic Speeds. NASA TM X-357, 1961.

9. Shanks, Robert E.: Investigation of the Low-Subsonic Stability and Control Characteristics of a Hypersonic Boost-Glide Type Airplane With Wing, Fuselage, and Vertical-Tail Modifications. NASA TM X-450, 1961.

L 1330

[redacted]

10. Hewes, Donald E.: Low-Subsonic Measurements of the Static and Oscillatory Lateral Stability Derivatives of a Sweptback-Wing Airplane Configuration at Angles of Attack From -10° to 90°. NASA MEMO 5-20-59L, 1959.

11. Campbell, John P., Johnson, Joseph L., Jr., and Hewes, Donald E.: Low-Speed Study of the Effect of Frequency on the Stability Derivatives of Wings Oscillating in Yaw With Particular Reference to High Angle-of-Attack Conditions. NACA RM L55H05, 1955.

TABLE I.- DIMENSIONAL CHARACTERISTICS OF MODEL

	Area, sq. in.	Span,* in.	Aspect ratio	Leading-edge sweep, deg	Trailing-edge sweep, deg	Dihedral, deg	$\bar{c}$, in.	Moment reference, in -	
								Percent $\bar{c}$	Percent l
W_8	1042.8	32.8	0.99	70	25	0	35.0	40.8	55.7
W_{8A}	971.6	32.8	1.07	70	36.8	0	32.3	40.3	55.7
W_{8B}	1162.8	32.8	.89	70	0	0	39.6	36.4	55.7
V_{10} (each)	95.3								
Fin	39.1			50					
Rudder	56.2			68					
Horizontal fin (each)	21.3			47					

*Measured to the theoretical wing tip.

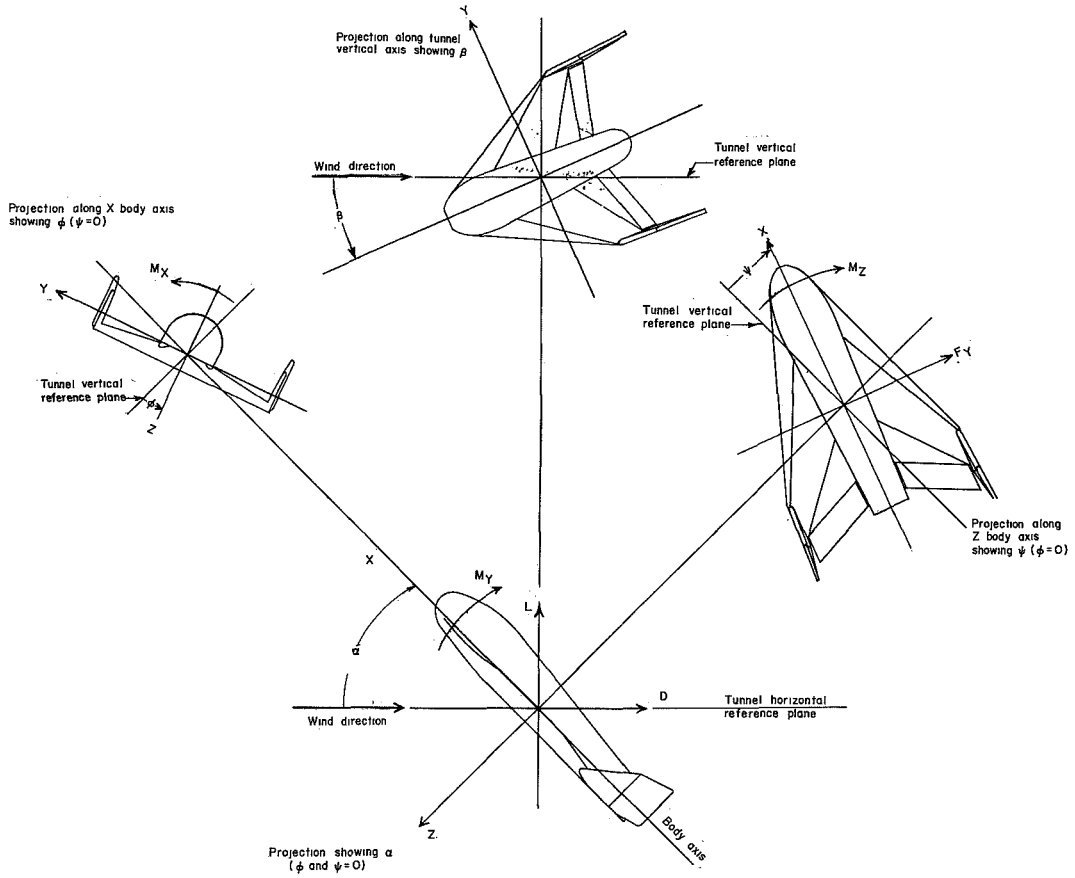

Figure 1.- Body system of axes. Arrows indicate positive directions of moments, forces, and angles. This system is defined as an orthogonal system having the origin at the center of gravity, and the X-axis is in the plane of symmetry and alined with the longitudinal axis of the fuselage. The Z-axis is in the plane of symmetry and perpendicular to the X-axis, and the Y-axis is perpendicular to the plane of symmetry.

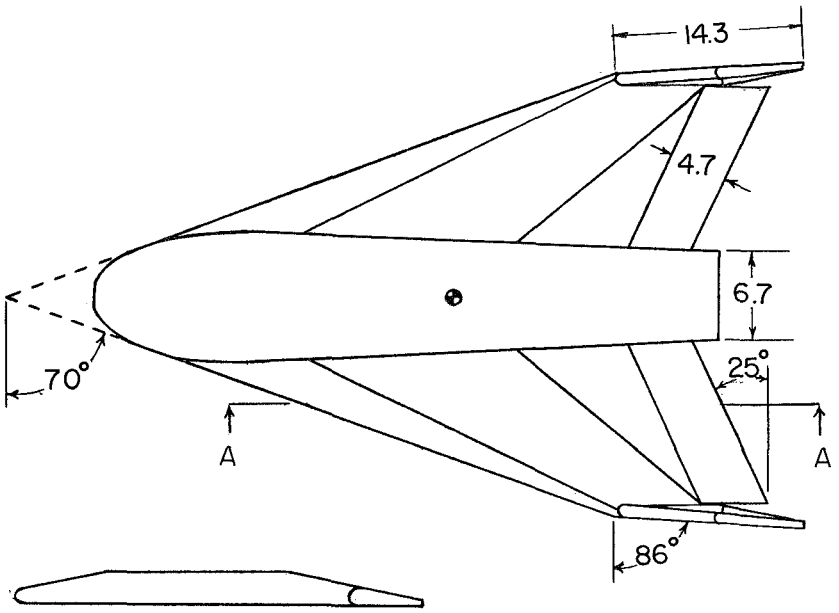

Section A – A

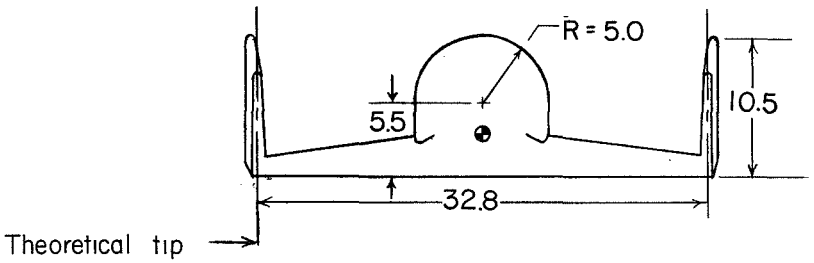

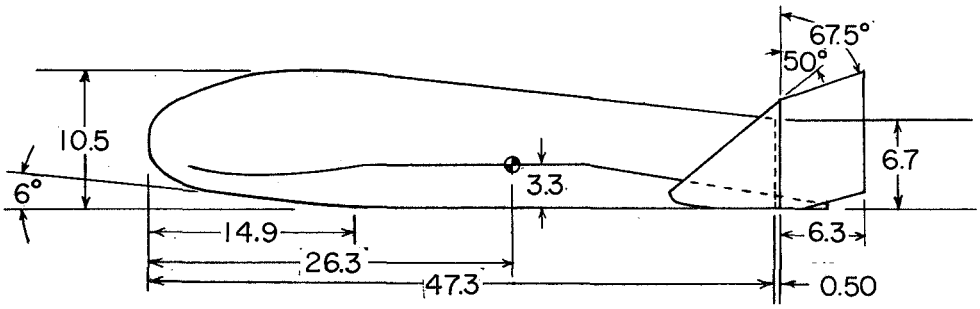

Figure 2.- Three-view drawing of model $B_8W_8V_{10}$ used in investigation. All dimensions are in inches.

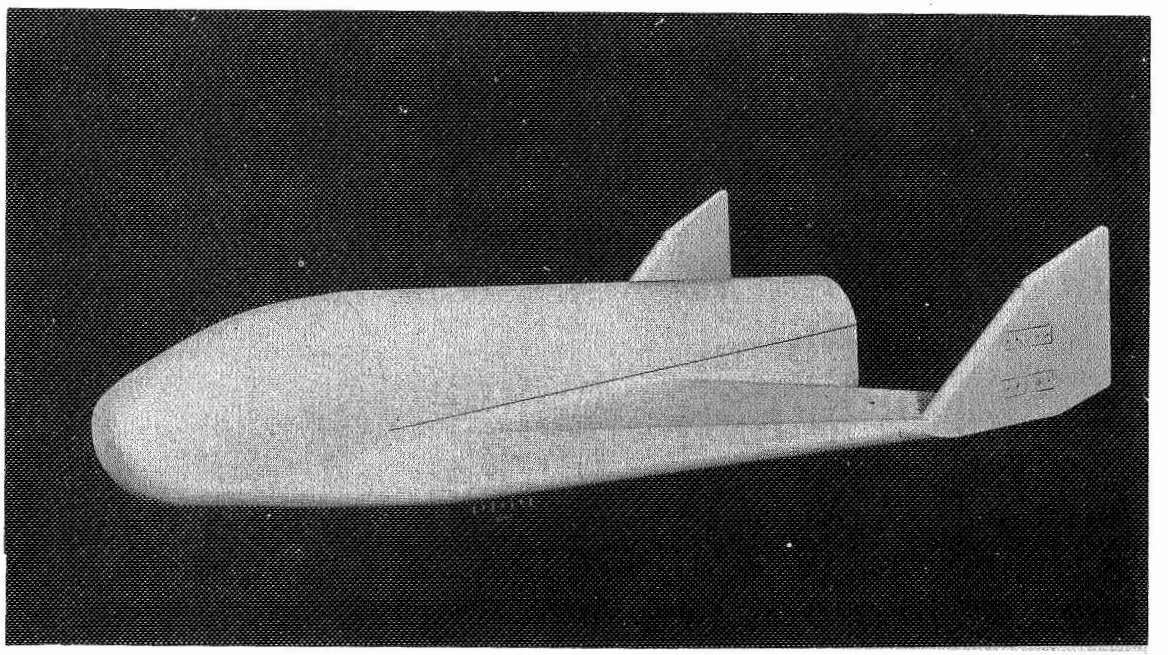

L-59-1525

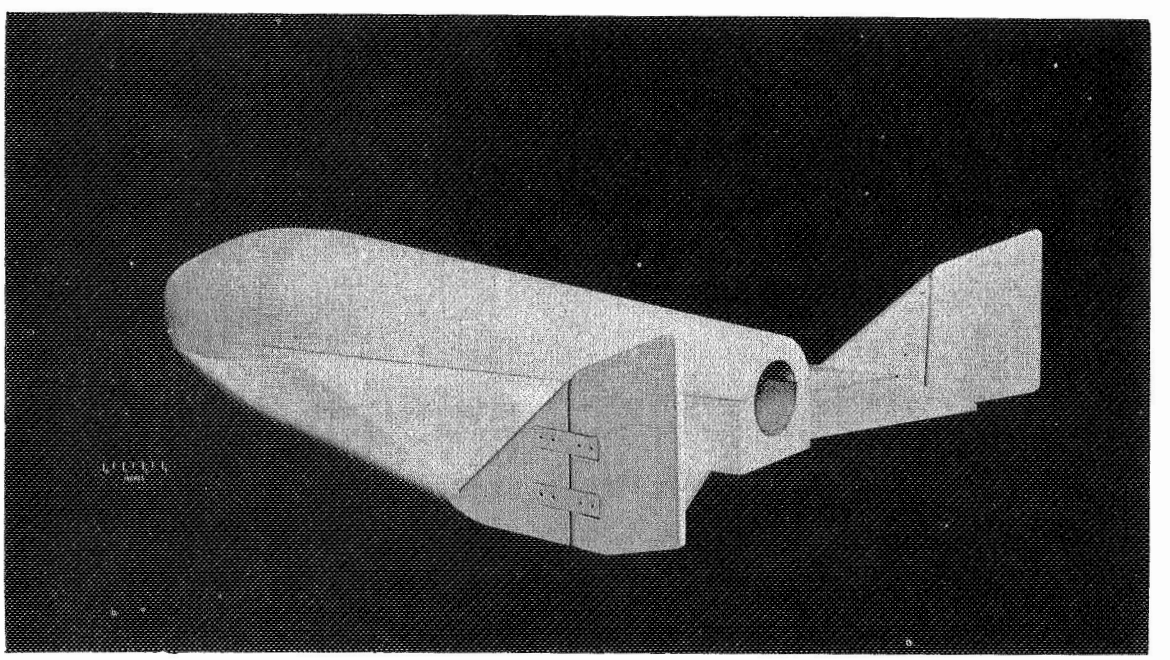

Figure 3.- Photographs of model used in investigation. L-59-1526

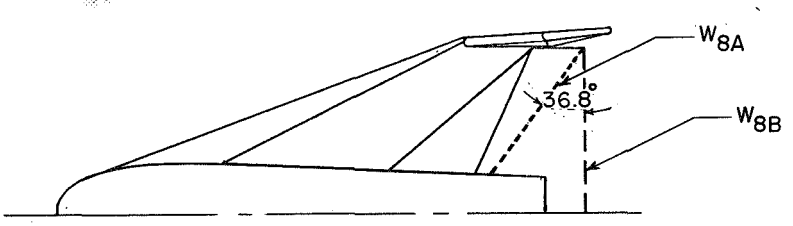

Wing trailing edge modification

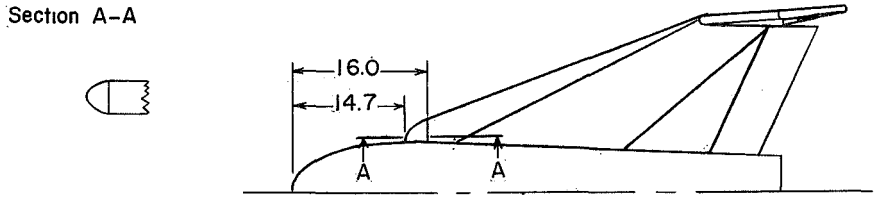

Wing leading-edge cutout

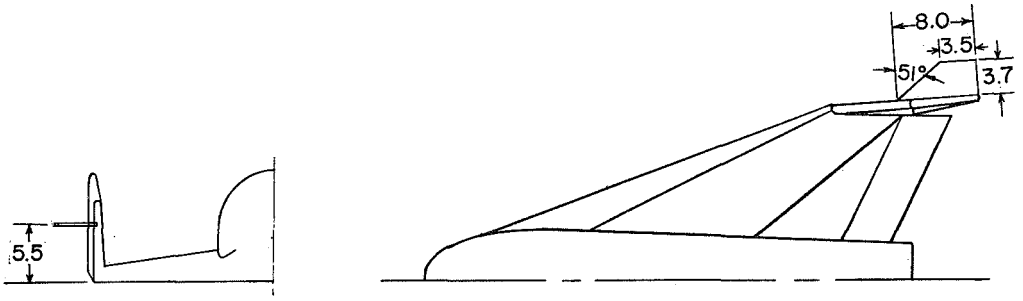

Horizontal fin

Landing skid

(a) Details of wing trailing-edge modifications, wing leading-edge cutout, horizontal fins, and landing skids.

Figure 4.- Modifications to the model. All dimensions are in inches.

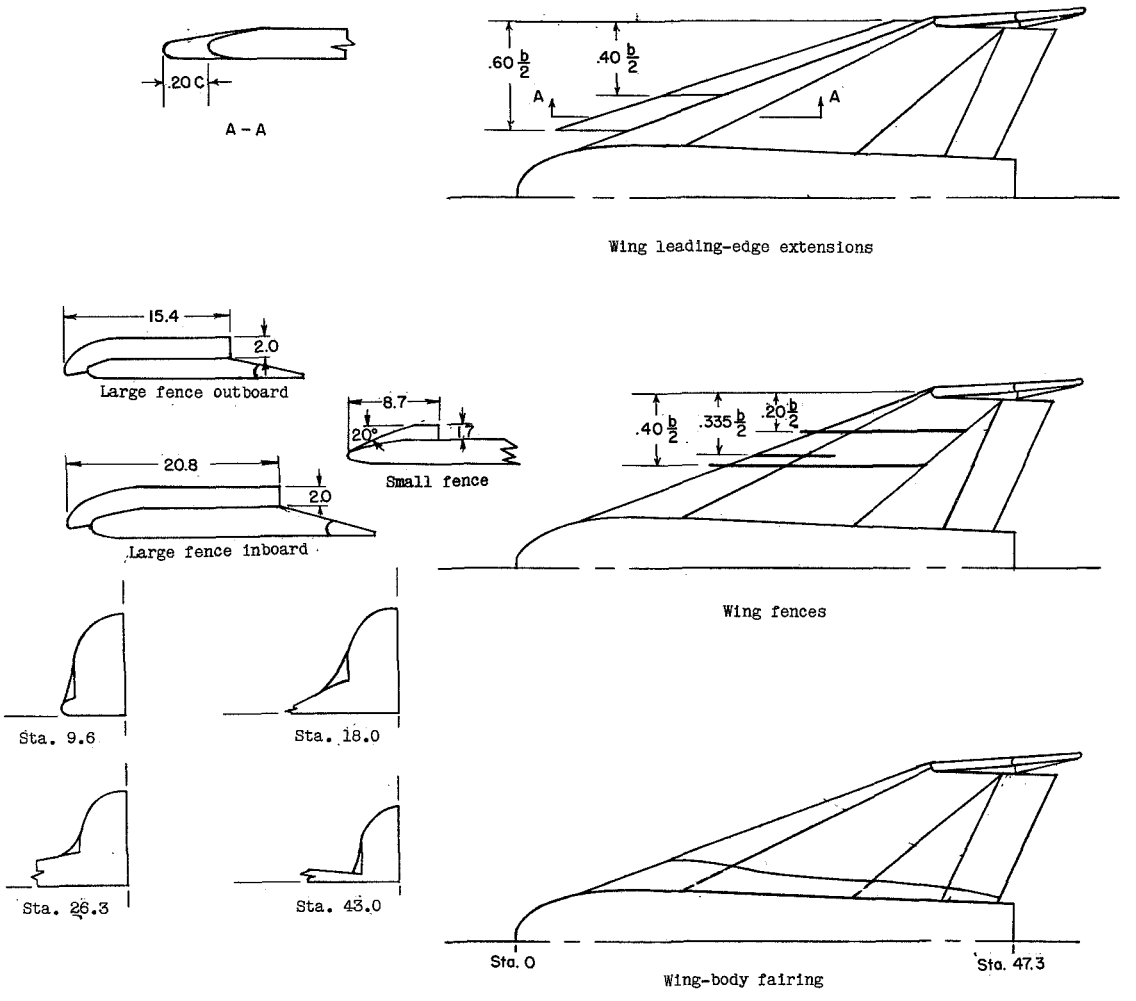

(b) Details of wing leading-edge extensions, wing fences, and wing-body fairing.

Figure 4.- Concluded.

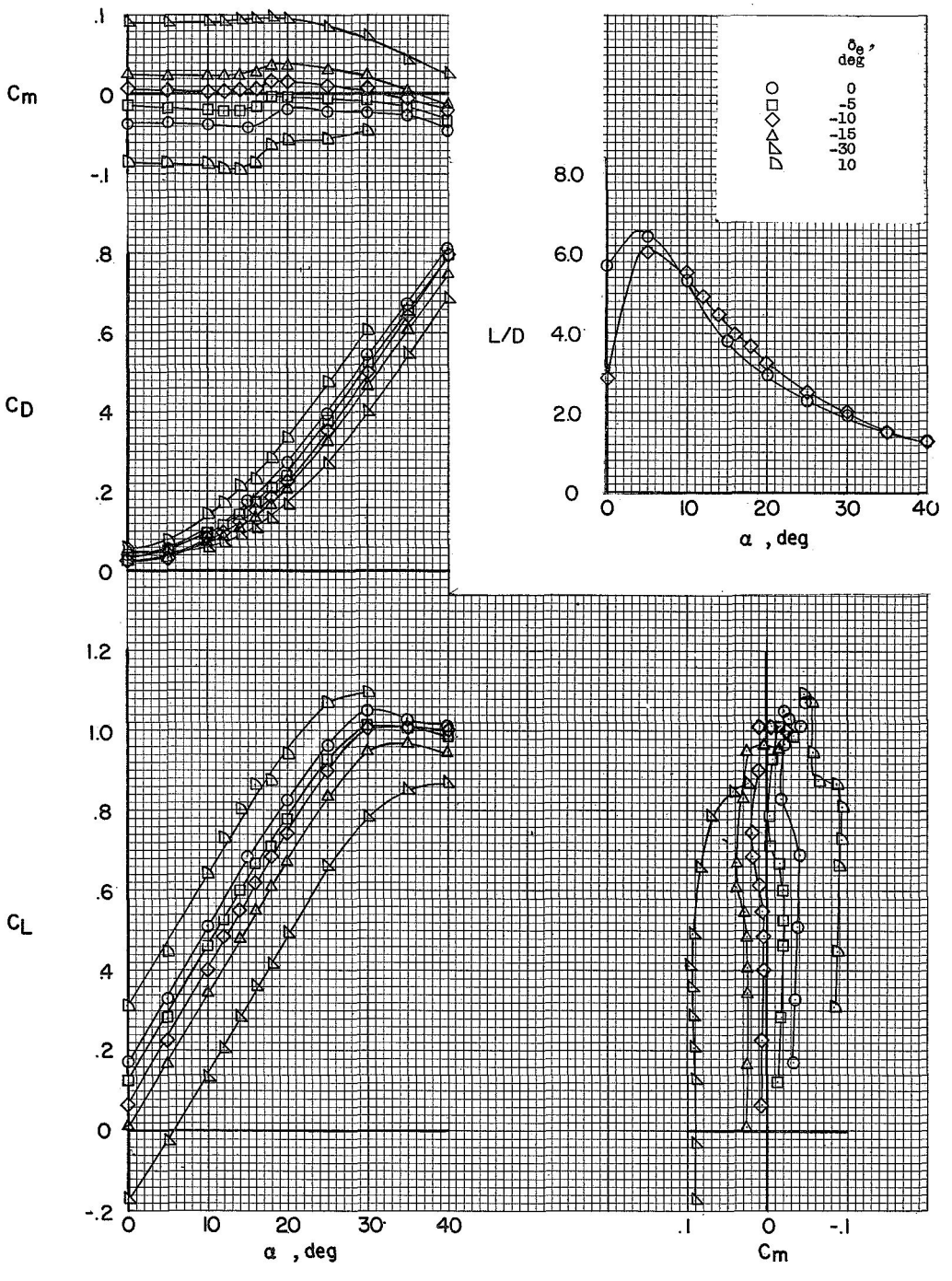

Figure 5.- Effect of elevator deflection on the static longitudinal characteristics of model $B_8W_8V_{10}$. $\beta = 0^o$.

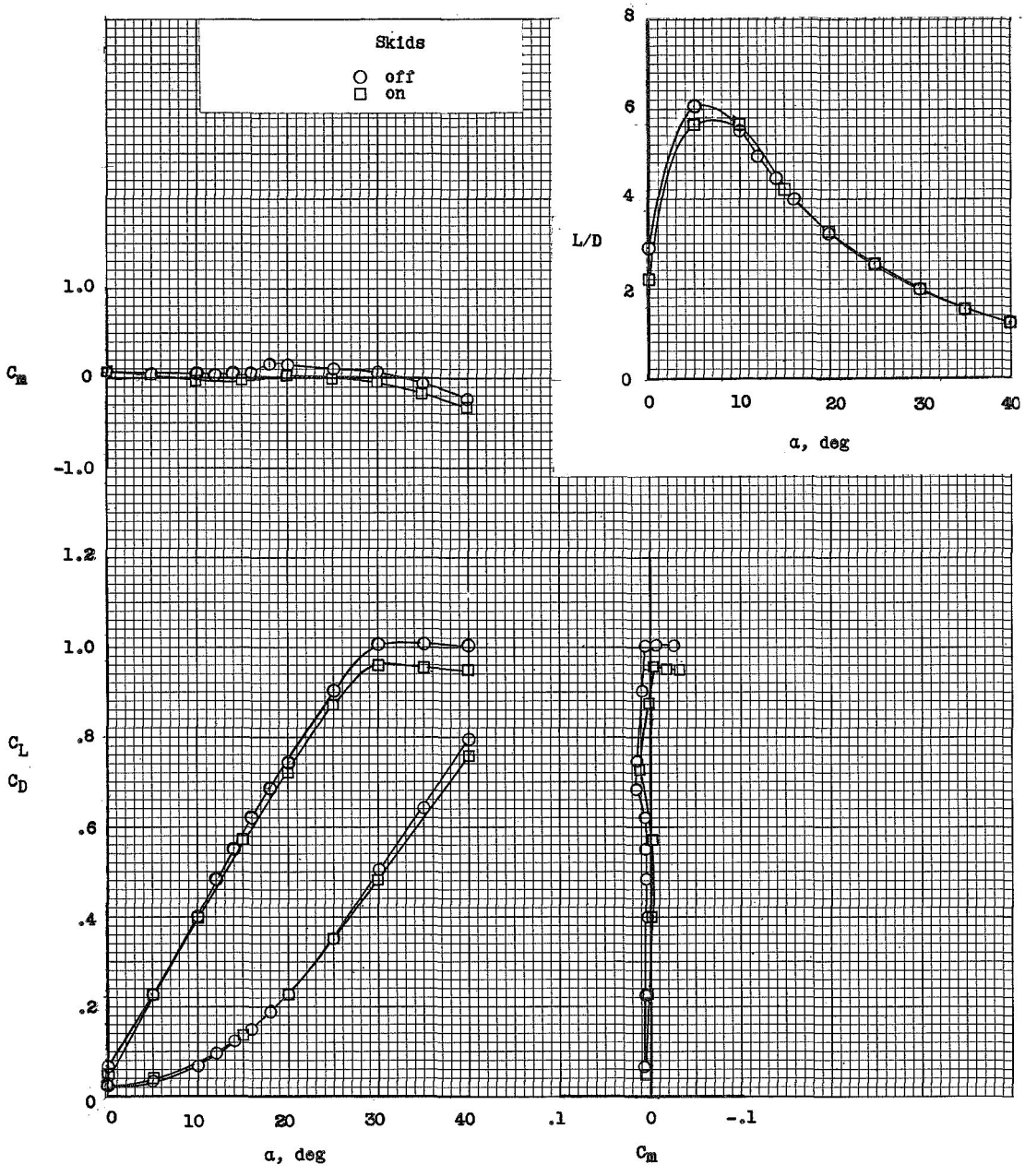

Figure 6.- Effects of landing skids on the static longitudinal characteristics of model $B_8W_8V_{10}$. $\delta_e = -10^\circ$; $\beta = 0^\circ$.

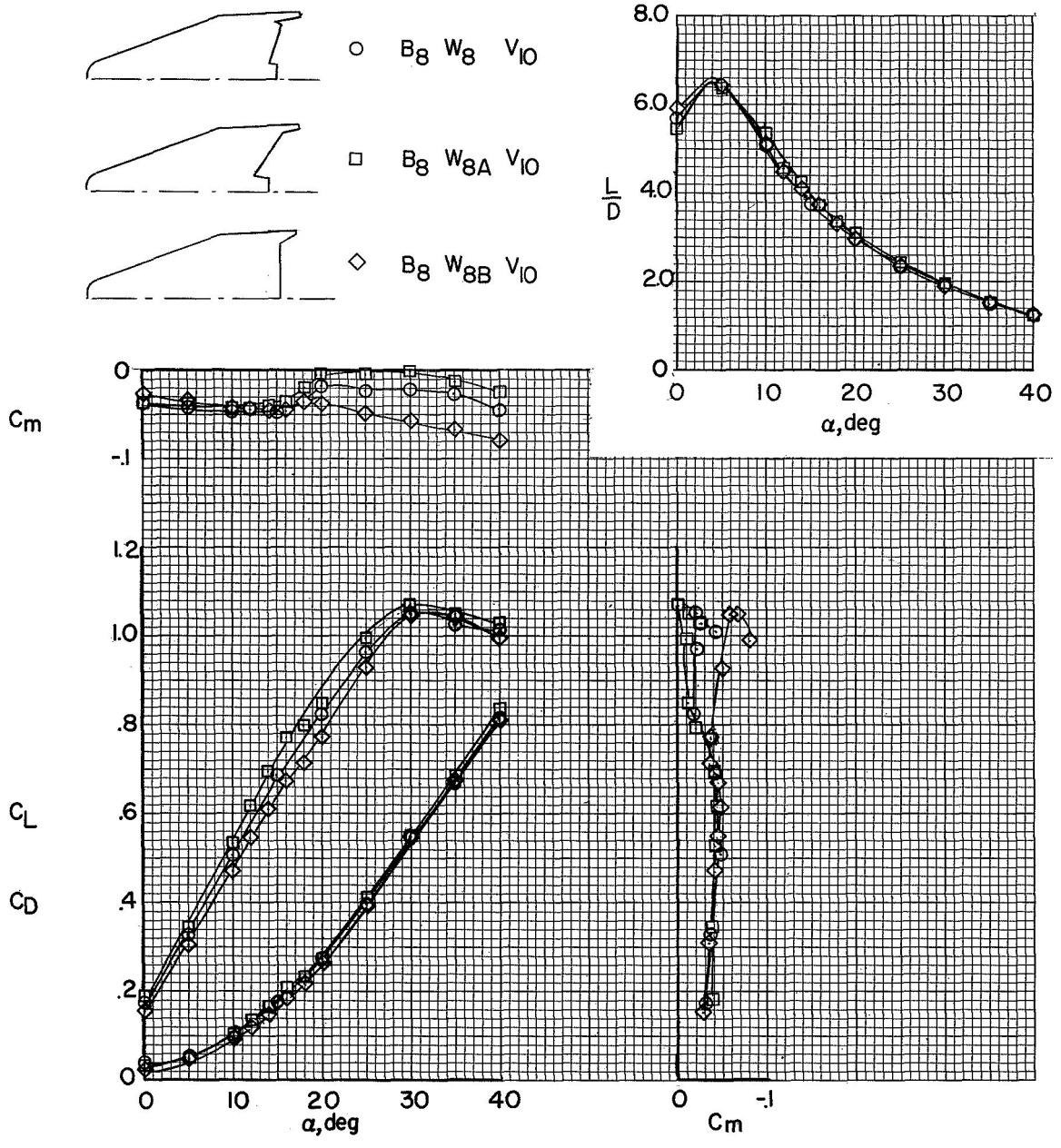

Figure 7.- Effect of wing trailing-edge configuration on the static longitudinal characteristics of model. $\beta = 0^{\circ}$; $\delta_e = 0^{\circ}$.

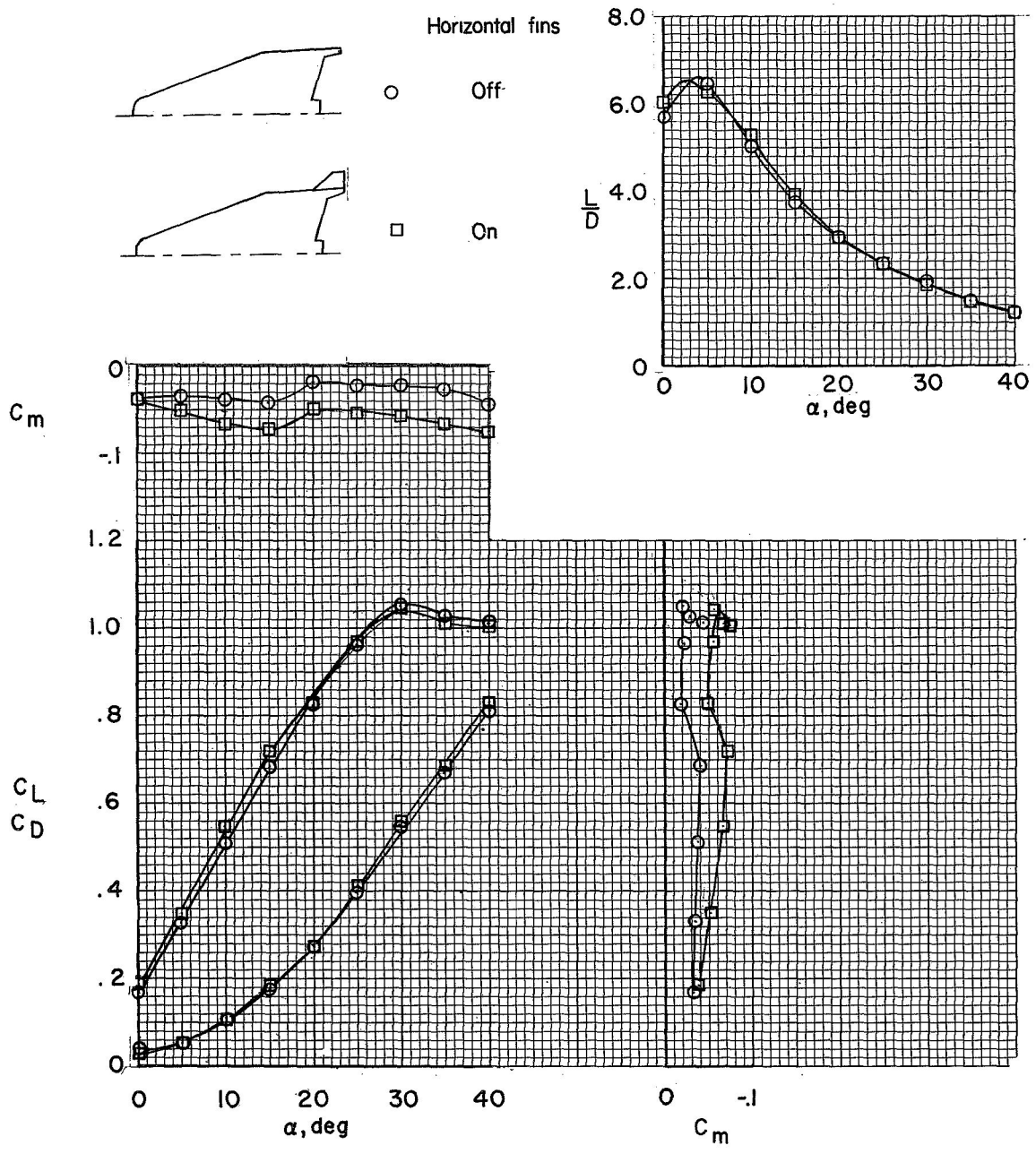

Figure 8.- Effect of horizontal fins on the static longitudinal characteristics of model $B_8W_8V_{10}$. $\beta = 0^\circ$; $\delta_e = 0^\circ$.

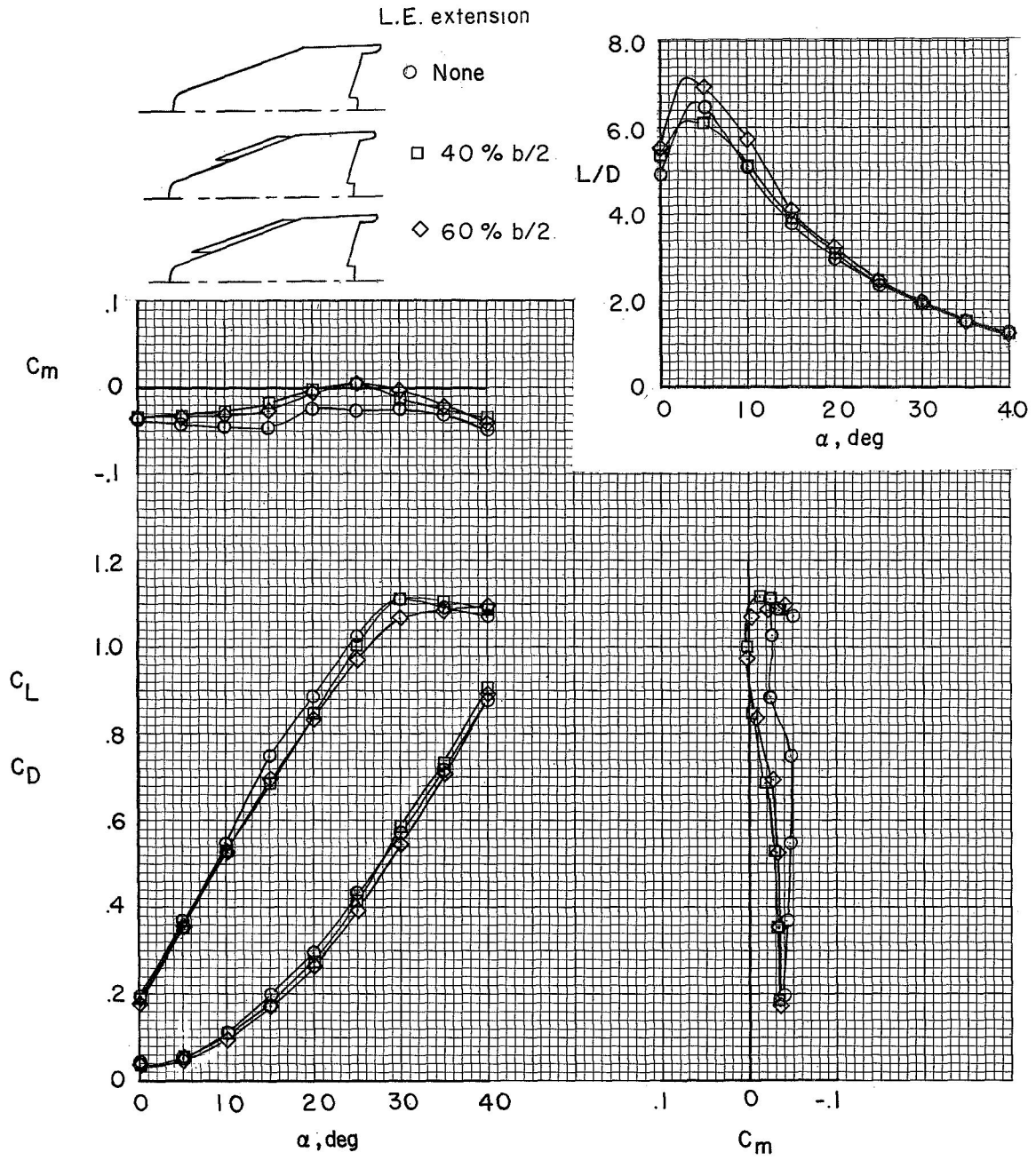

Figure 9.- Effect of leading-edge extensions on the static longitudinal characteristics of model $B_8W_8V_{10}$. $\beta = 0^\circ$; $\delta_e = 0^\circ$.

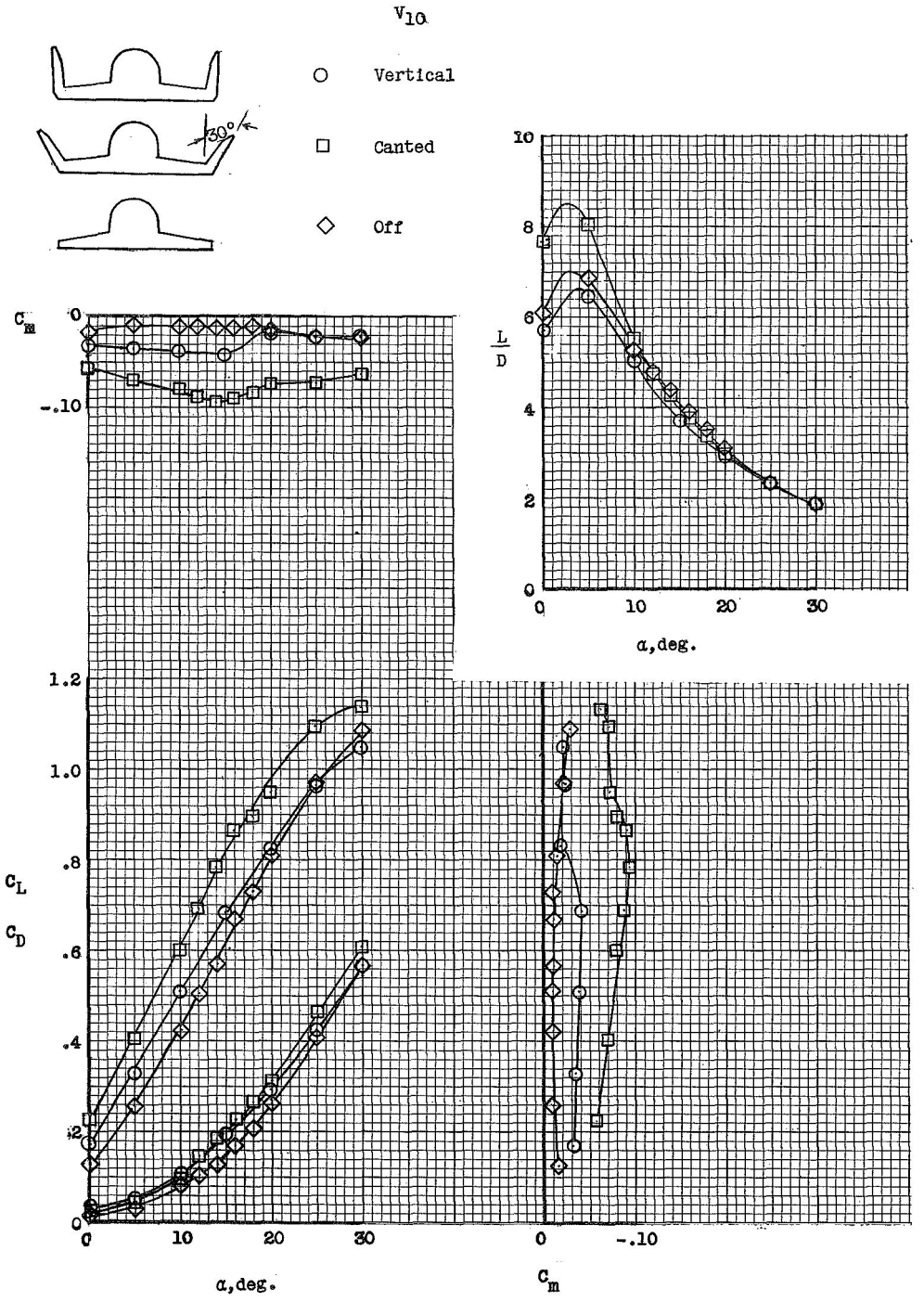

Figure 10.- Effect of vertical tails and vertical-tail cant on static longitudinal characteristics of model B_8W_8. $\beta = 0^\circ$; $\delta_e = 0^\circ$.

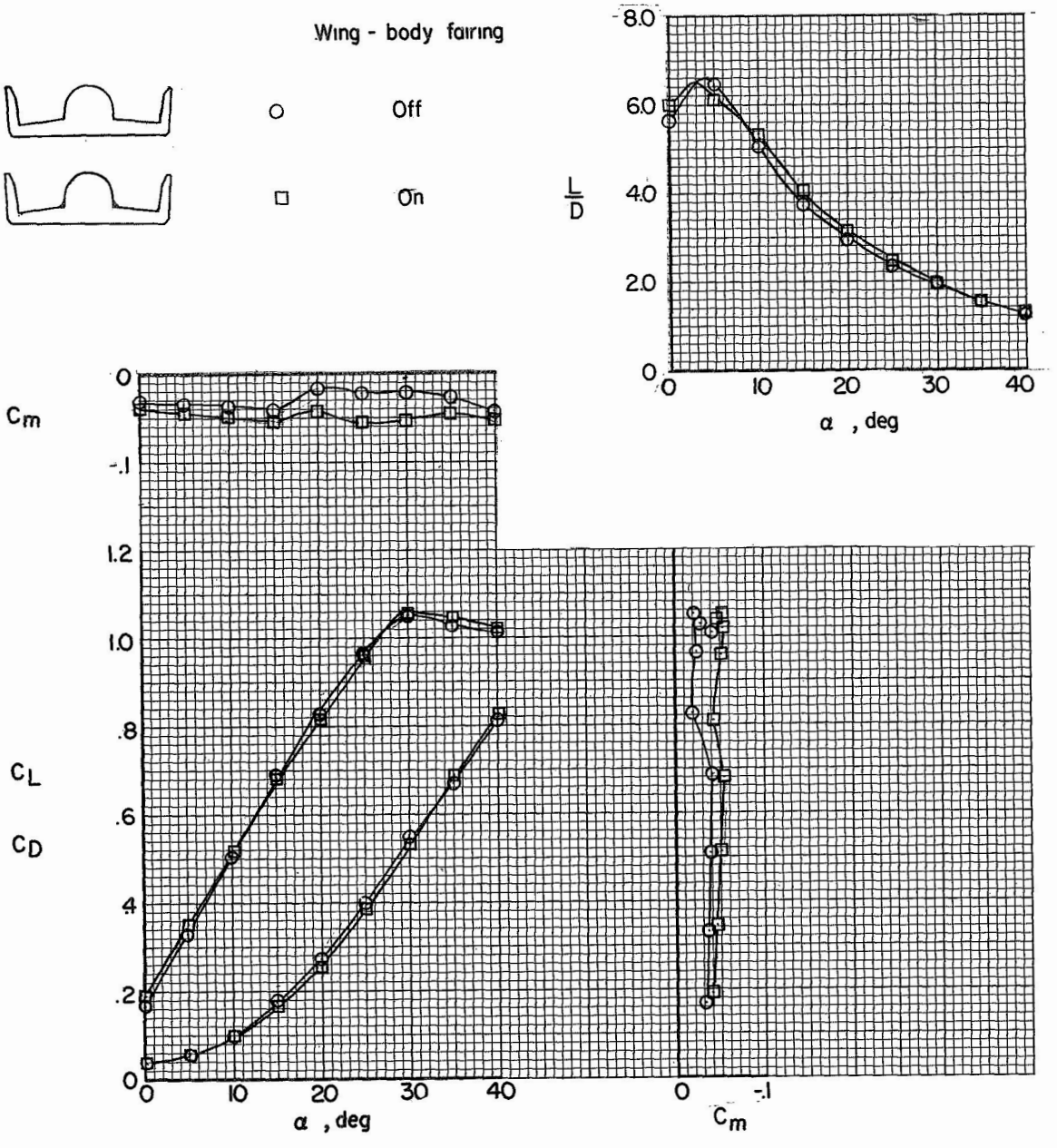

Figure 11.- Effect of wing-body fairing on longitudinal characteristics of model $B_8W_8V_{10}$. $\beta = 0^\circ$; $\delta_e = 0^\circ$.

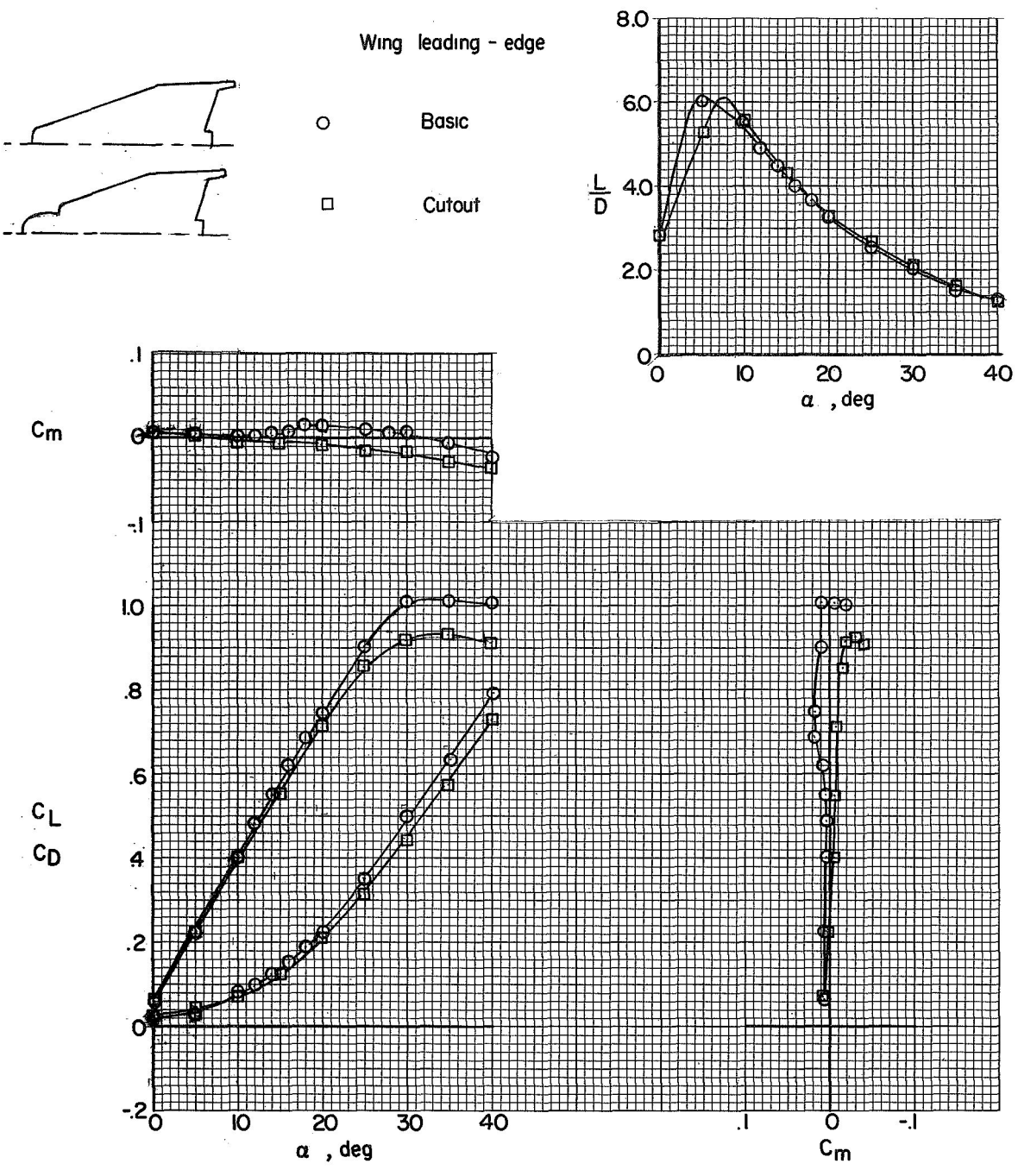

I-1330

Figure 12.- Effect of wing leading-edge cutout on longitudinal characteristics of model. $\beta = 0^{\circ}$; $\delta_e = -10^{\circ}$.

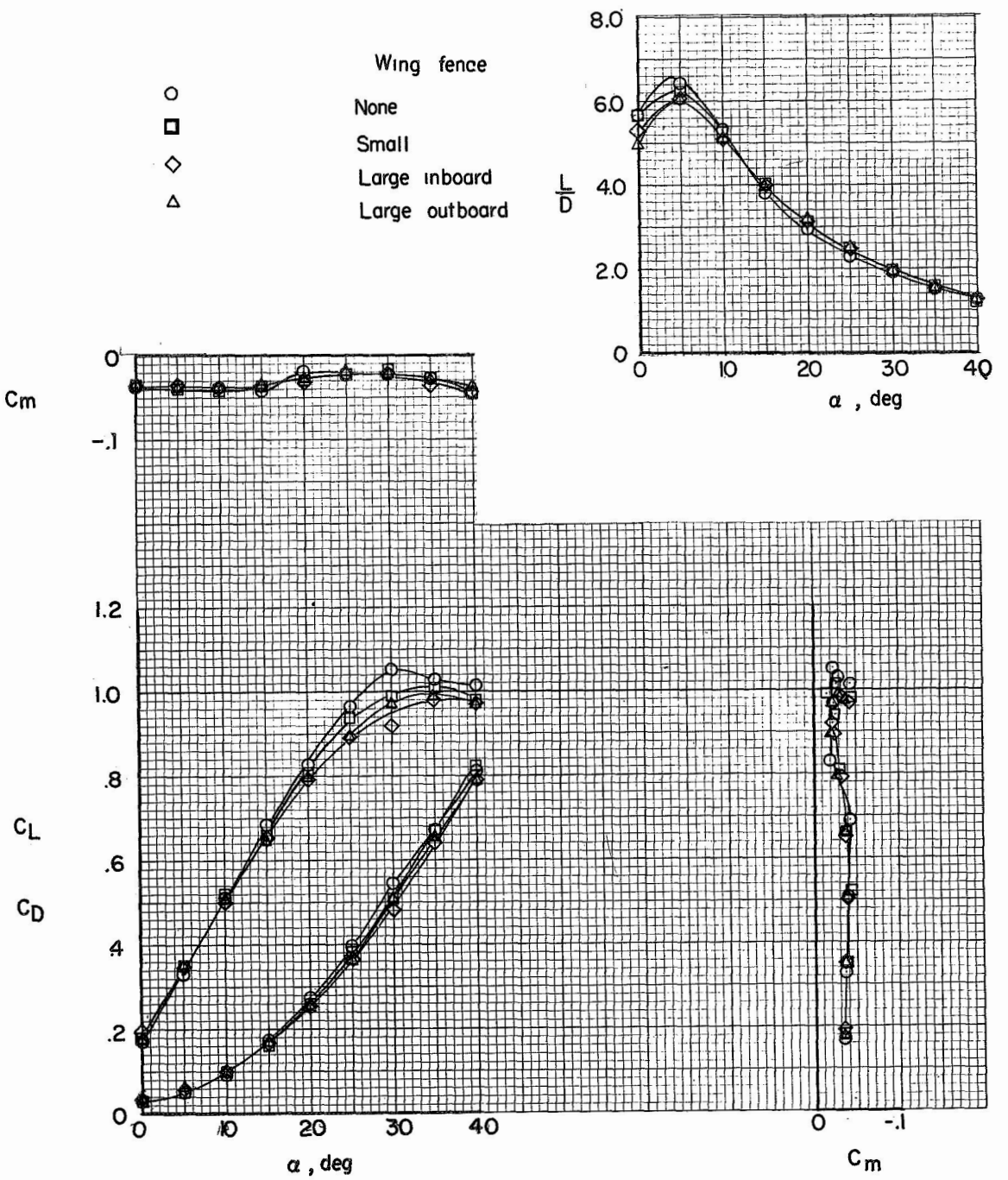

Figure 13.- Effect of wing fences on the static longitudinal characteristics of model $B_8W_8V_{10}$. $\beta = 0^\circ$; $\delta_e = 0^\circ$.

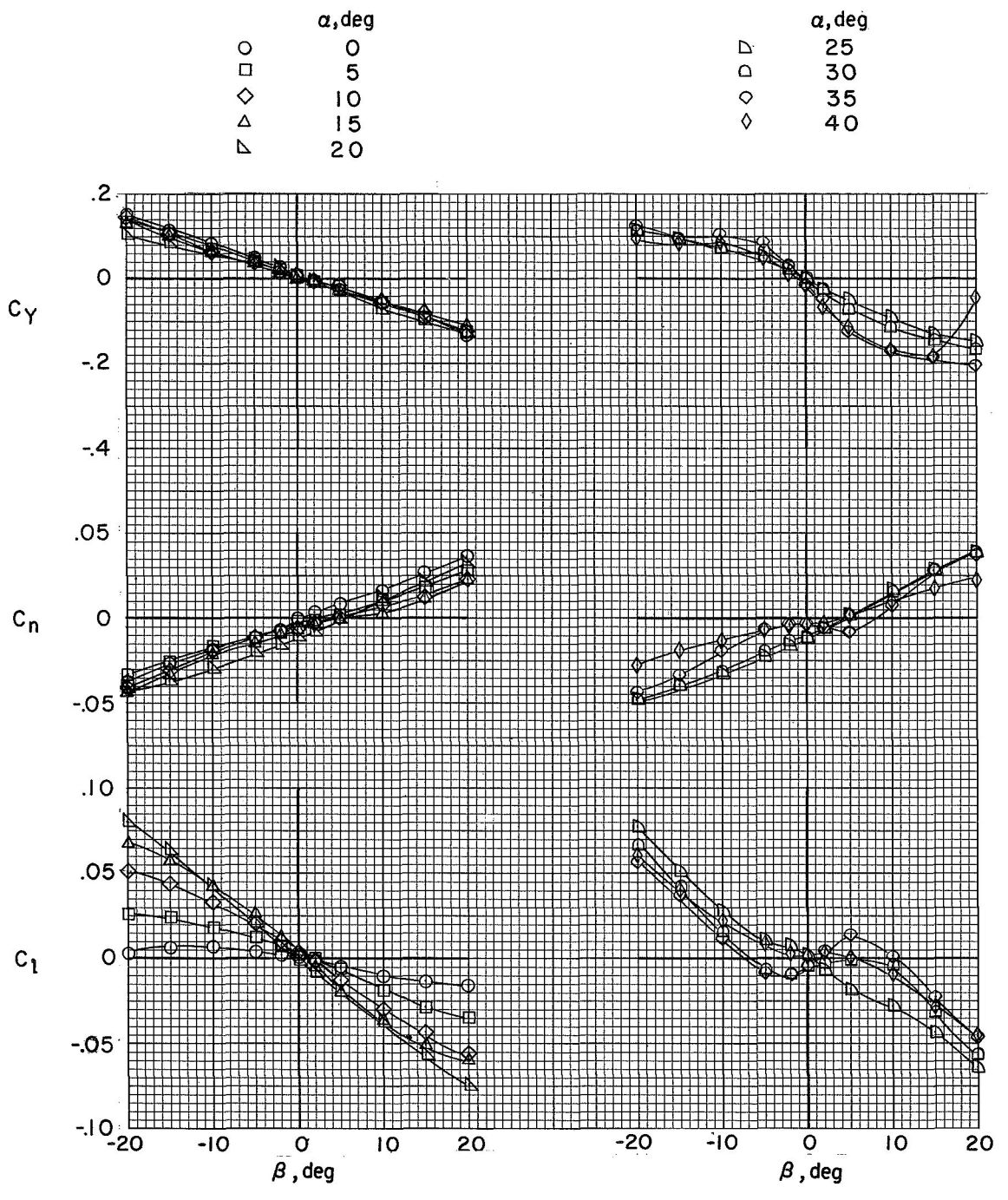

(a) Vertical tails on.

Figure 14.- Variation of lateral coefficients of model $B_8W_8V_{10}$ with angle of sideslip. $\delta_e = -10^\circ$.

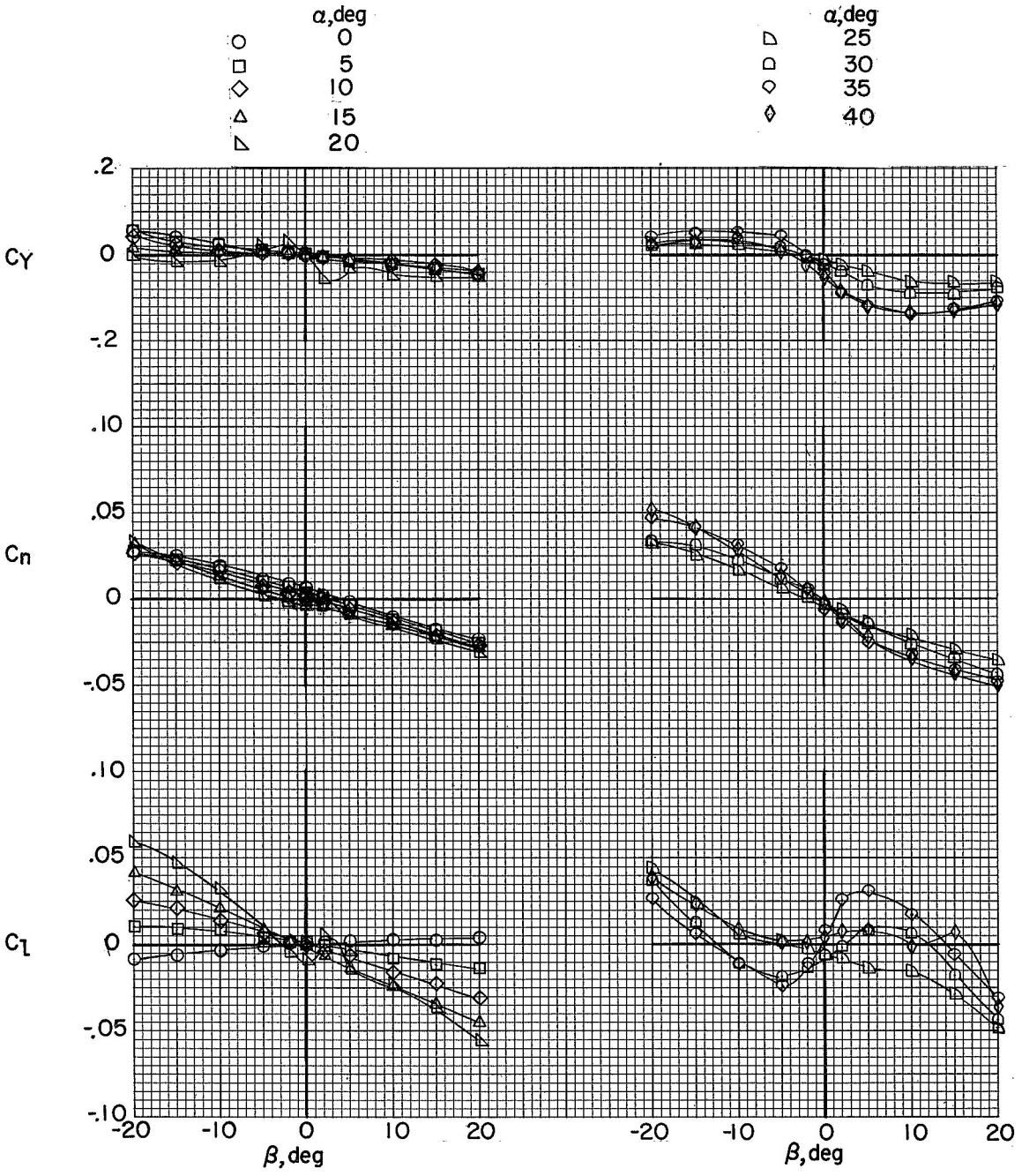

(b) Vertical tails off.

Figure 14.- Continued.

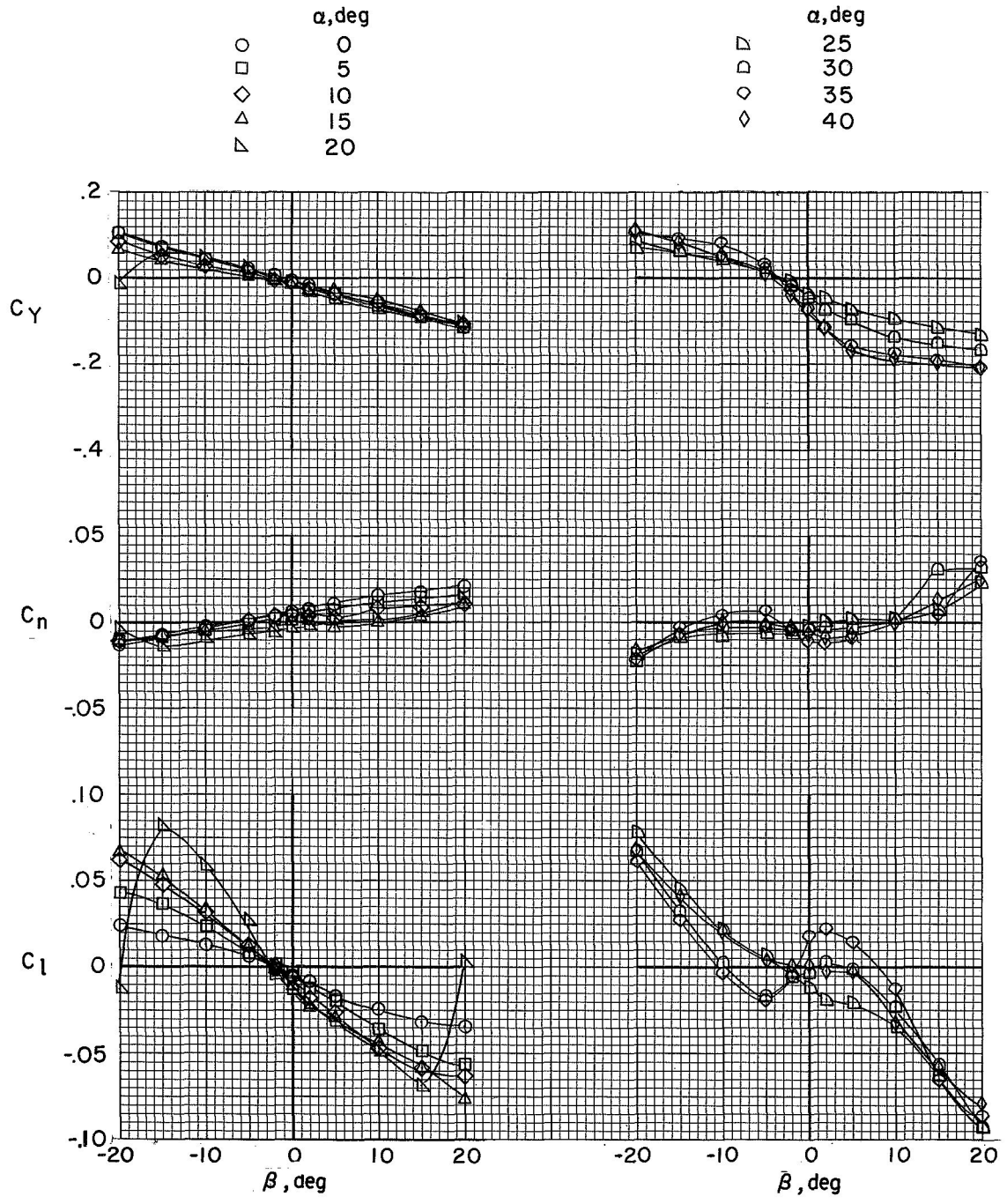

(c) Tails canted out 30° from vertical.

Figure 14.- Continued.

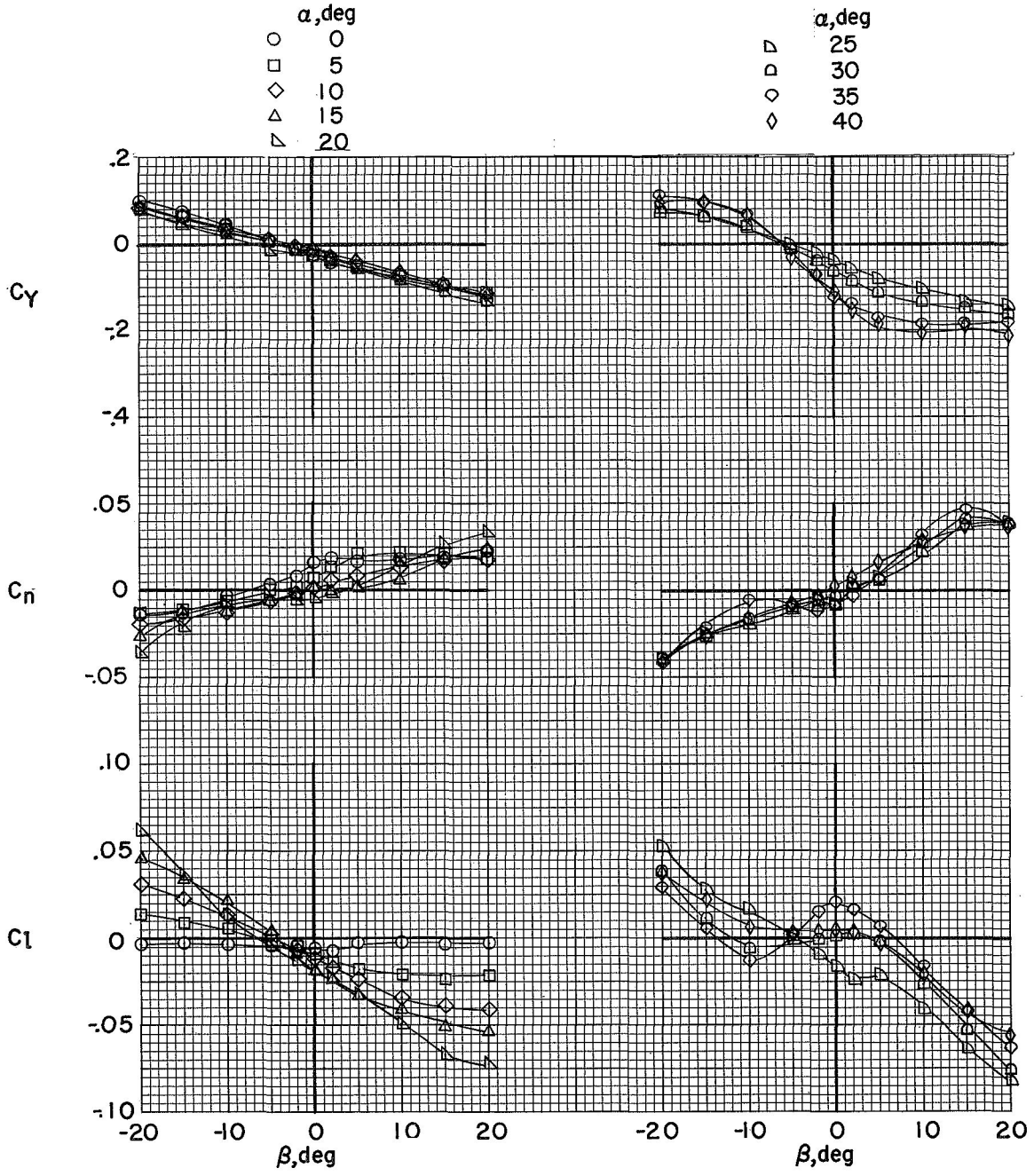

(d) Rudders deflected 20° outward.

Figure 14.- Continued.

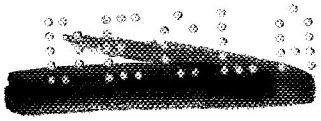

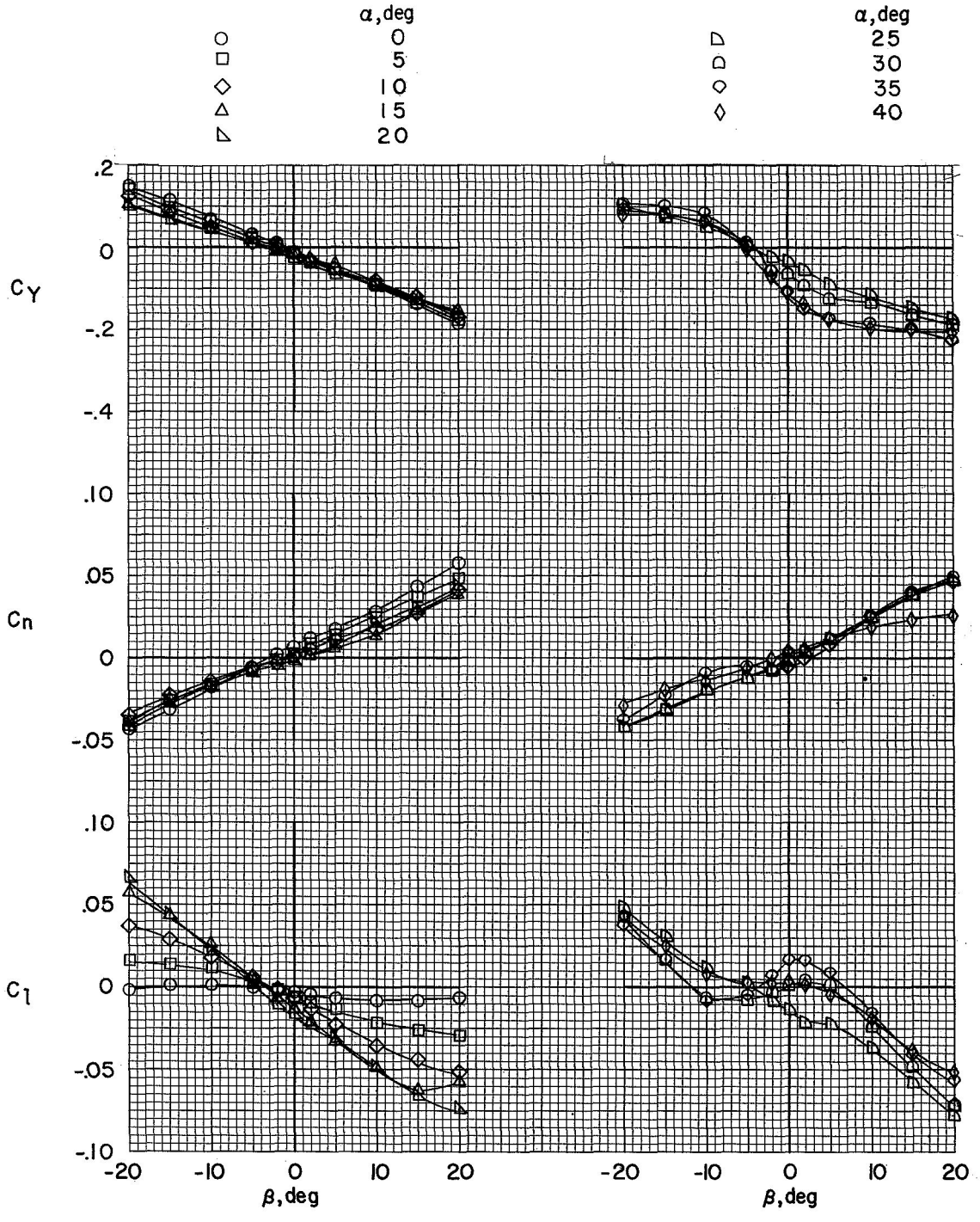

(e) $B_8W_8V_{10}$ with landing skids.

Figure 14.- Concluded.

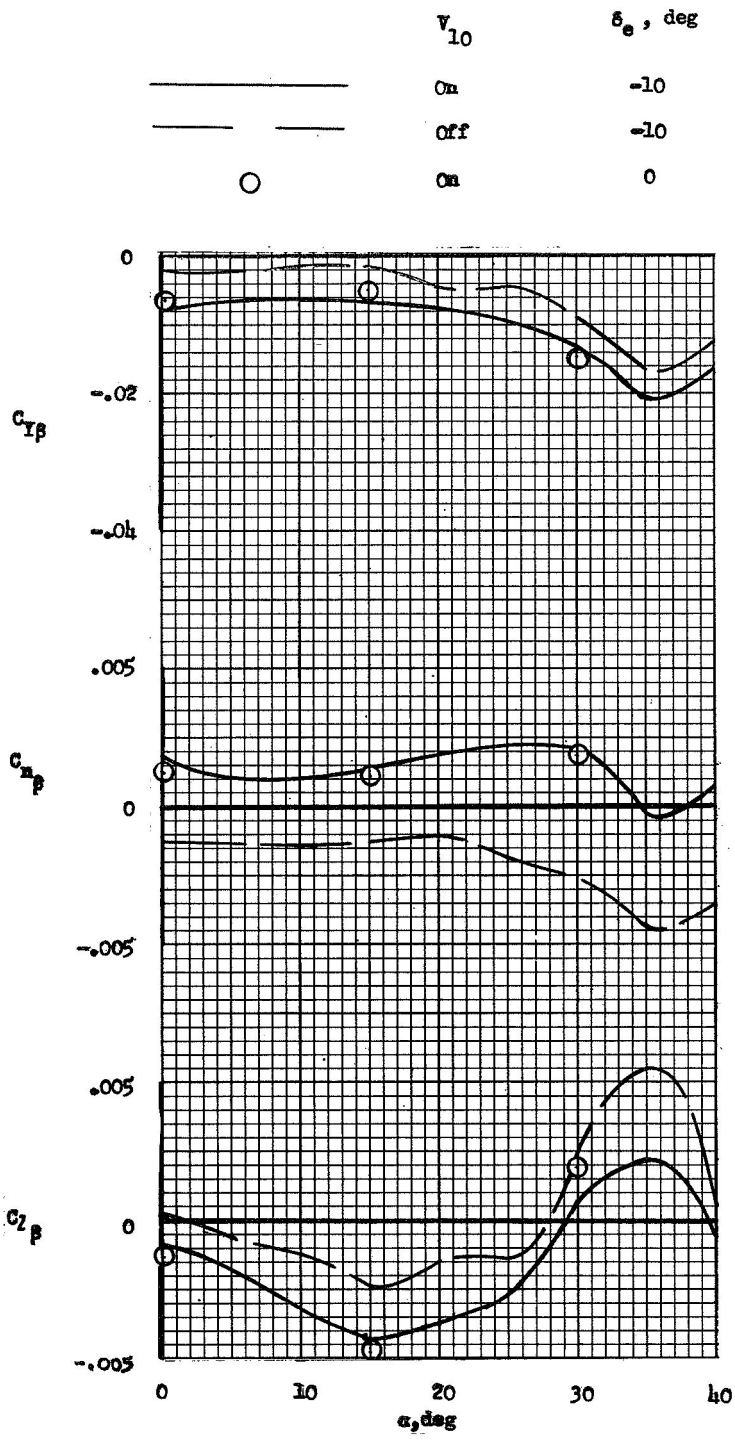

Figure 15.- Effect of vertical tails on the static lateral characteristics of model B_8W_8.

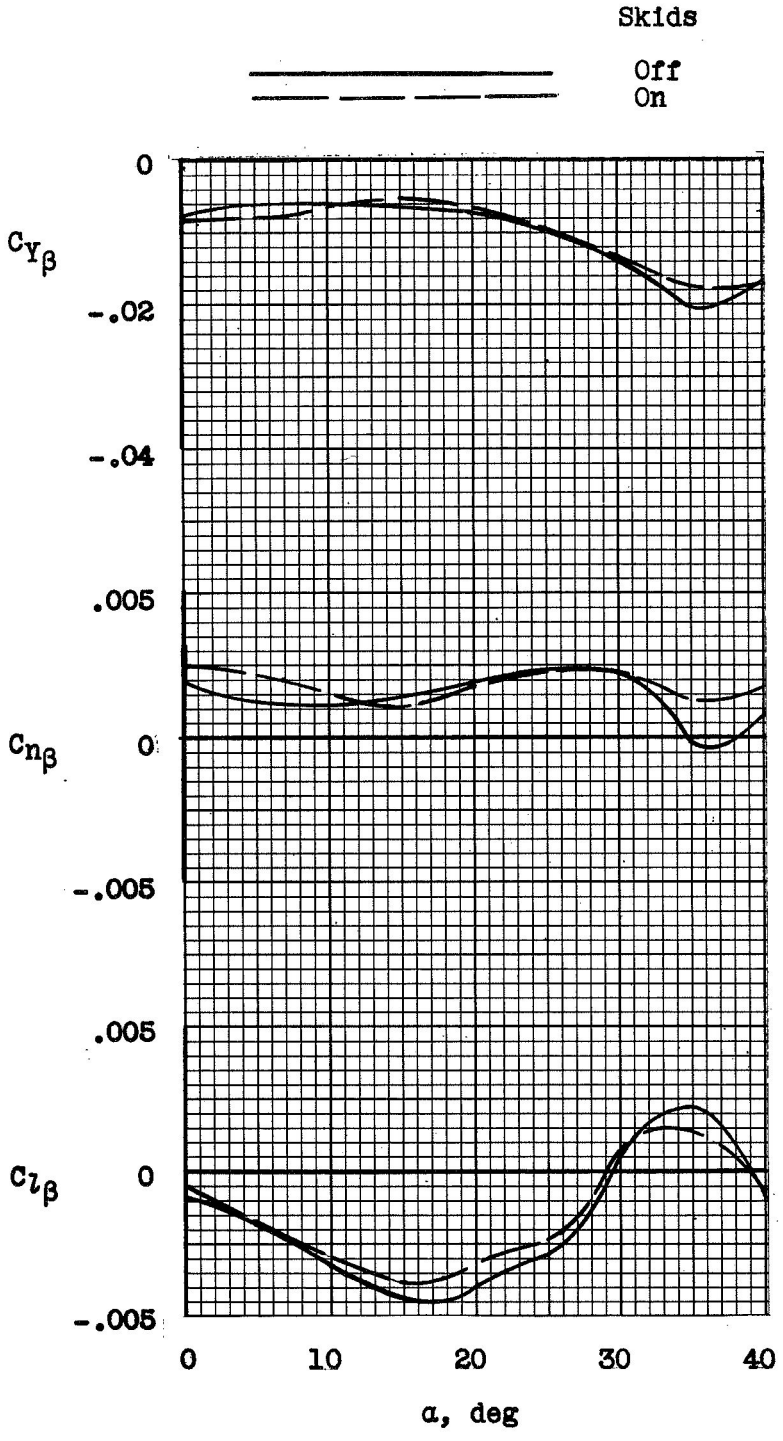

Figure 16.- Effect of landing skids on the static lateral characteristics of model $B_8W_8V_{10}$. $\delta_e = -10^\circ$.

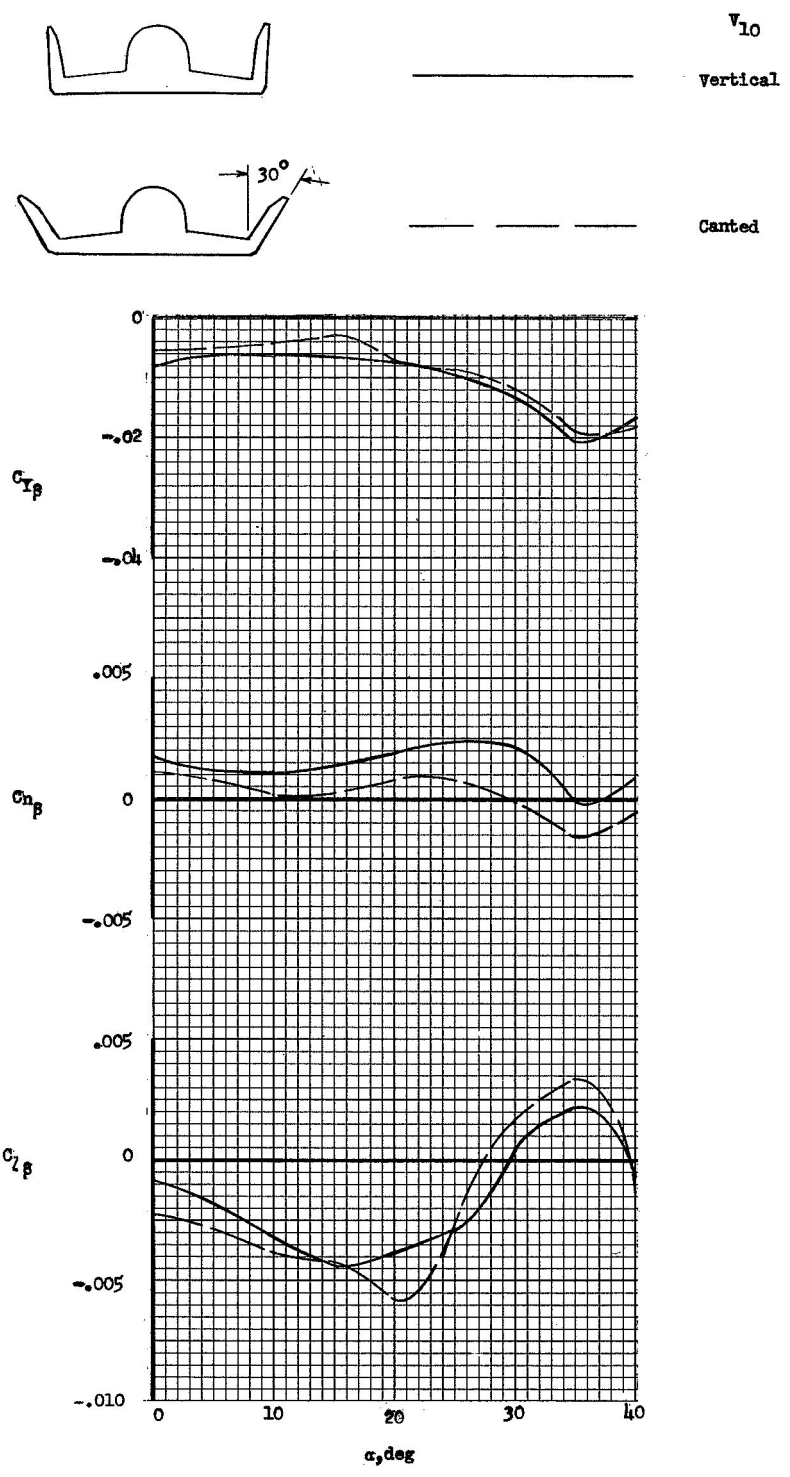

Figure 17.- Effect of vertical tail cant on the static lateral characteristics of model $B_8W_8V_{10}$. $\delta_e = -10^\circ$.

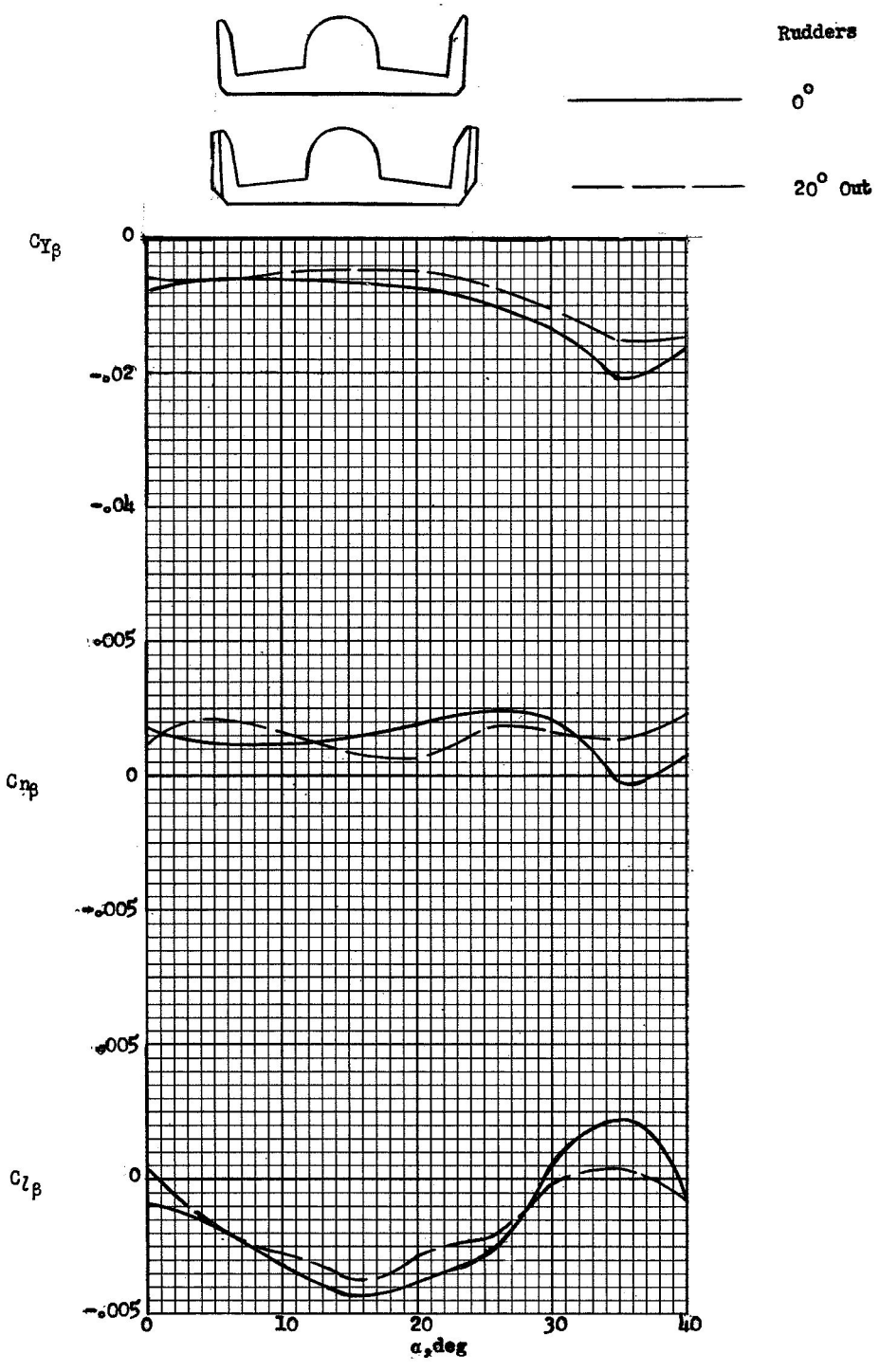

Figure 18.- Effect of rudders deflected 20° outward on the static lateral characteristics of model $B_8W_8V_{10}$. $\delta_e = -10°$.

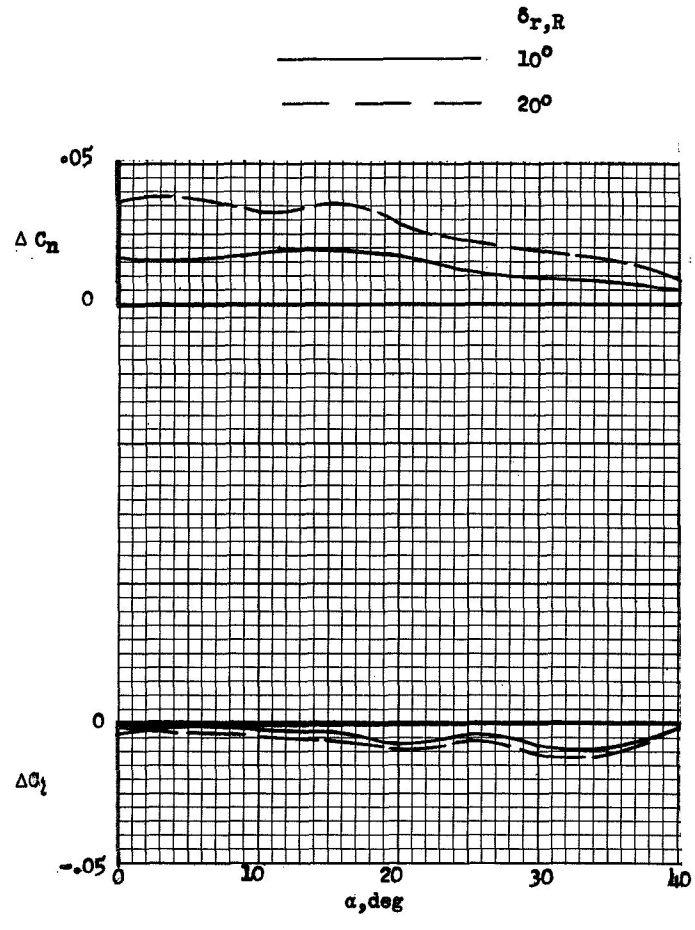

(a) Rudder.

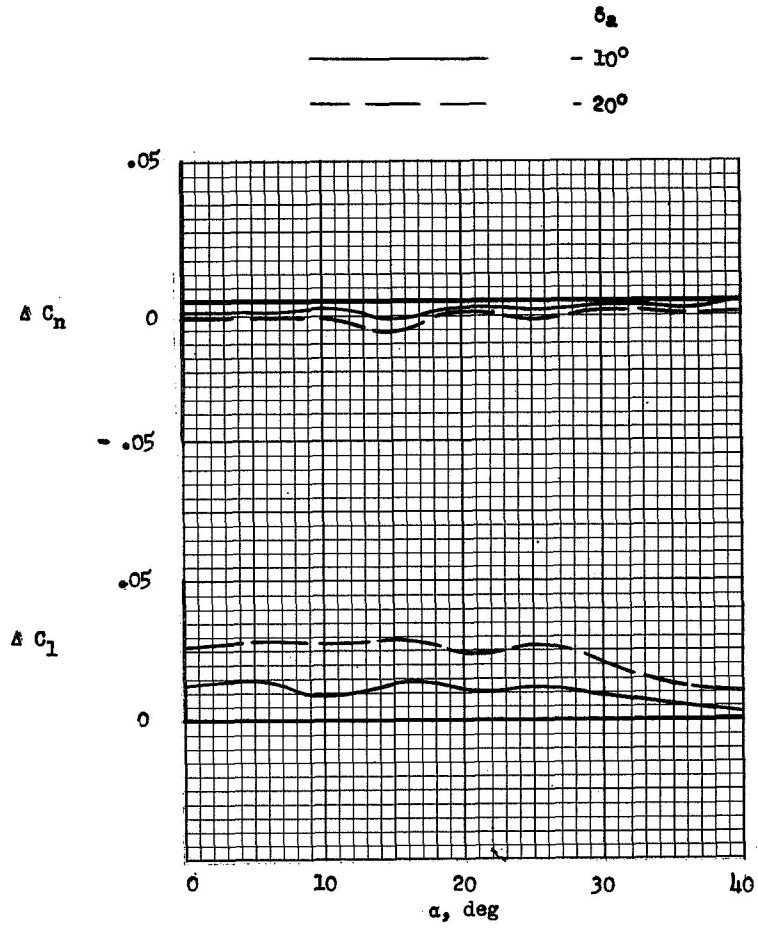

(b) Aileron.

Figure 19.- Rudder and aileron effectiveness of model $B_8W_8V_{10}$. $\delta_e = -10^\circ$.

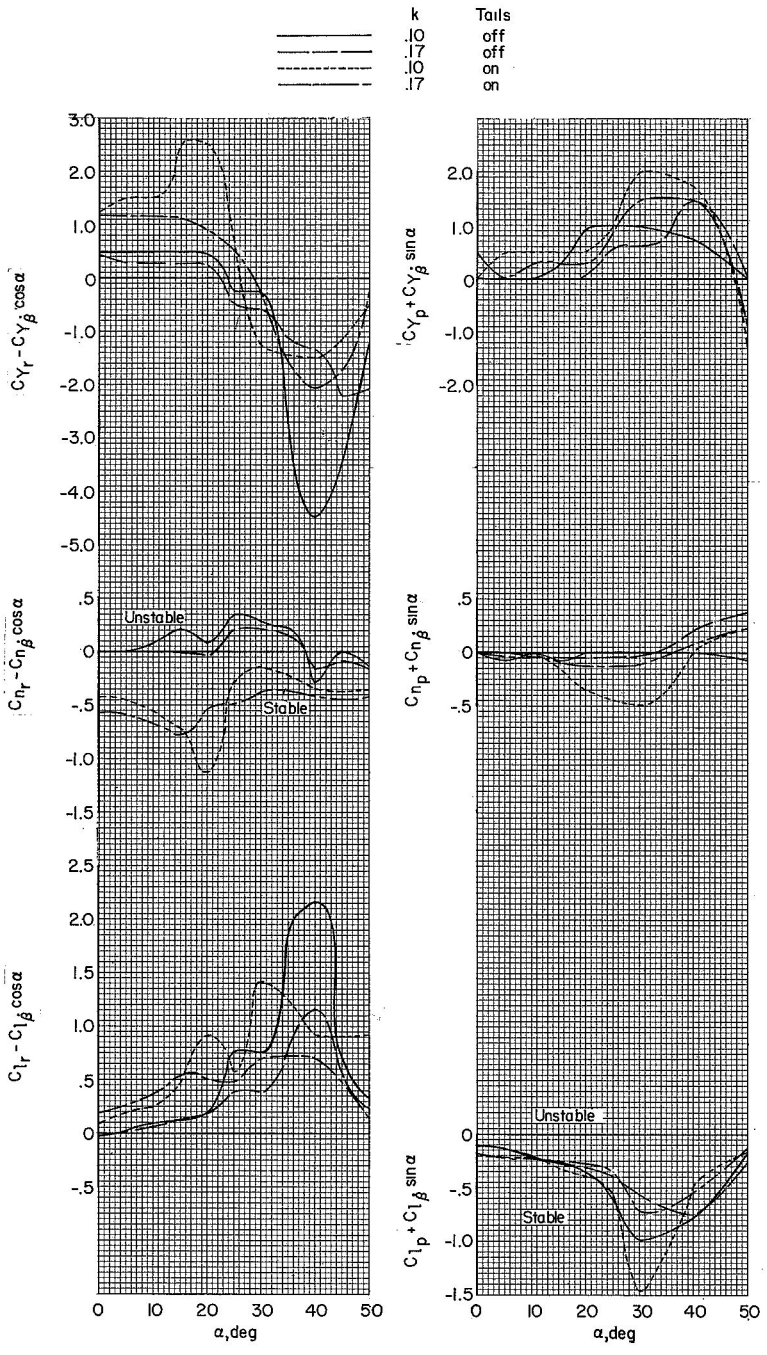

(a) Yawing. (b) Rolling.

Figure 20.- Variation of the out-of-phase yawing and rolling derivatives with angle of attack for model $B_8W_8V_{10}$. $\delta_e = 0^\circ$ per radian.

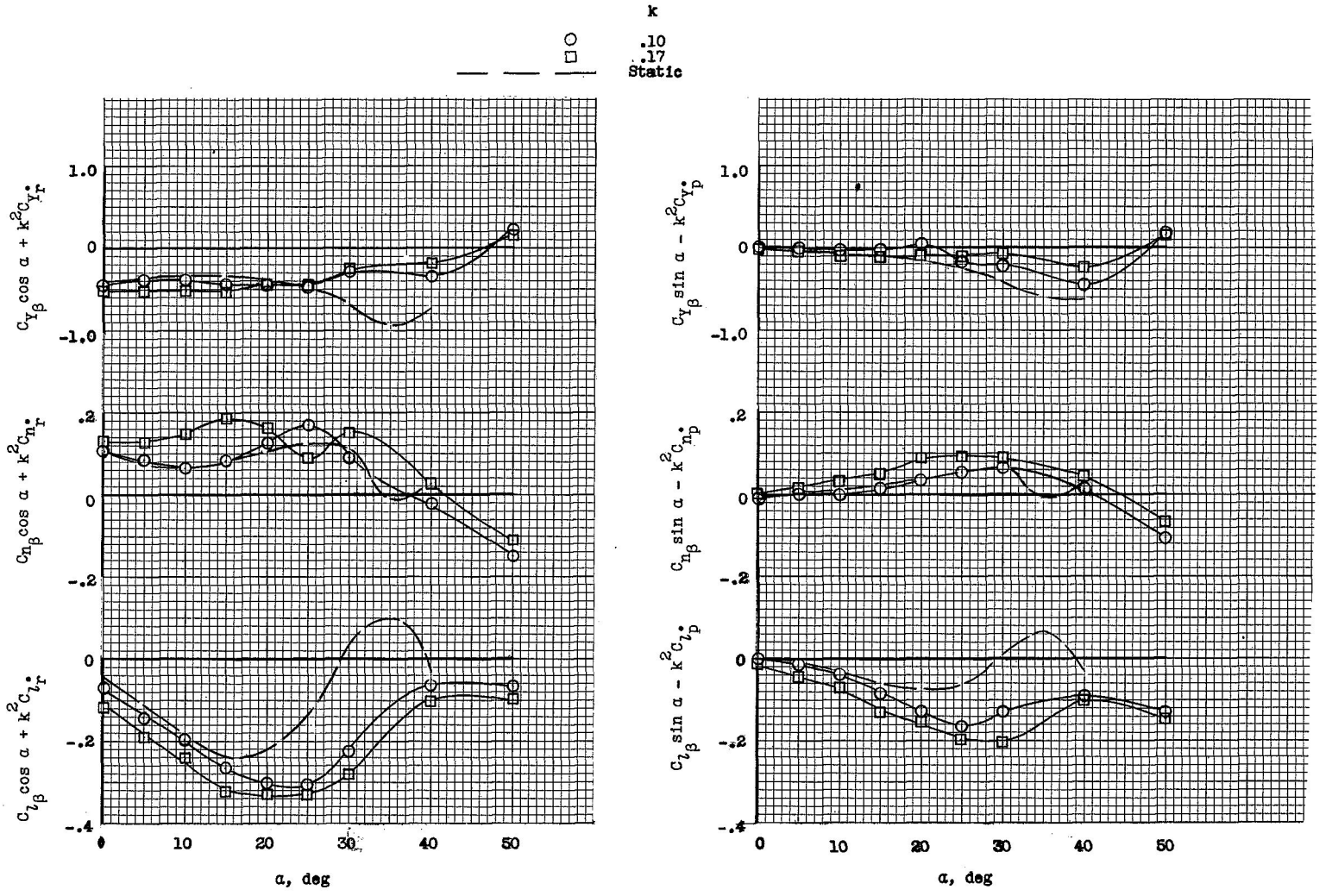

(a) Yawing.

(b) Rolling.

Figure 21.- Variation of in-phase-with-displacement yawing and rolling derivatives with angle of attack for model $B_8W_8V_{10}$. $\delta_e = 0^\circ$ per radian.